AUTHOR QUERY FORM

ELSEVIER	**Journal: VOLGEO** **Article Number: 5460**	**Please e-mail or fax your responses and any corrections to:** **Sundarababu, Anitha** **E-mail: Corrections.ESCH@elsevier.spitech.com** **Fax: +1 619 699 6721**

Dear Author,

Please check your proof carefully and mark all corrections at the appropriate place in the proof (e.g., by using on-screen annotation in the PDF file) or compile them in a separate list. Note: if you opt to annotate the file with software other than Adobe Reader then please also highlight the appropriate place in the PDF file. To ensure fast publication of your paper please return your corrections within 48 hours.

For correction or revision of any artwork, please consult http://www.elsevier.com/artworkinstructions.

We were unable to process your file(s) fully electronically and have proceeded by

☐ Scanning (parts of) your article ☐ Rekeying (parts of) your article ☐ Scanning the artwork

Any queries or remarks that have arisen during the processing of your manuscript are listed below and highlighted by flags in the proof. Click on the 'Q' link to go to the location in the proof.

Location in article	**Query / Remark: click on the Q link to go** **Please insert your reply or correction at the corresponding line in the proof**
Q1	The citation "Blundy and Cashmann (2001)" has been changed to match the author name/date in the reference list. Please check here and in subsequent occurrences, and correct if necessary.
Q2	Please check the layout and table header in Table 1 and amend if necessary.
Q3	Your article is registered as a regular item and is being processed for inclusion in a regular issue of the journal. If this is NOT correct and your article belongs to a Special Issue/Collection please contact a.sundarababu@elsevier.com immediately prior to returning your corrections.
Q4	Please check the capturing of the author affiliations and amend if necessary.
Q5, Q8	This sentence has been slightly modified for clarity. Please check that the meaning is still correct, and amend if necessary.
Q6	The number of keywords provided exceeds the maximum allowed by this journal. Please delete 1 keyword.
Q7	Citation "Magyari et al., 2014" has not been found in the reference list. Please supply full details for this reference.
Q9	The citation "Radulescu, 1988" has been changed to match the author name/date in the reference list. Please check here and in subsequent occurrences, and correct if necessary.
Q10	Uncited references: This section comprises references that occur in the reference list but not in the body of the text. Please position each reference in the text or, alternatively, delete it. Thank you.
Q11	Please check the captured grant sponsors and amend if necessary.
Q12	Please provide an update for reference "Magyari et al., in press".

Q13	Please confirm that given names and surnames have been identified correctly.

Please check this box if you have no corrections to make to the PDF file. ☐

Thank you for your assistance.

Journal of Volcanology and Geothermal Research xxx (2014) xxx

Contents lists available at ScienceDirect

Journal of Volcanology and Geothermal Research

journal homepage: www.elsevier.com/locate/jvolgeores

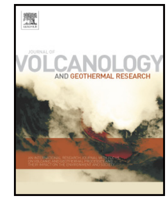

Highlights

Journal of Volcanology and Geothermal Research xxx (2014) xxx–xxx

Combined magnetotelluric and petrologic constrains for the nature of the magma storage system beneath the Late Pleistocene Ciomadul volcano (SE Carpathians)

S. Harangi [a,b,*], A. Novák [c], B. Kiss [a,d], I. Seghedi [e], R. Lukács [a,d], L. Szarka [c], V. Wesztergom [c], M. Metwaly [f], K. Gribovszki [c]

[a] *MTA-ELTE Volcanology Research Group, H-1117 Budapest, Pázmány sétány 1/C, Budapest, Hungary*
[b] *Department of Petrology and Geochemistry, Eötvös University, Budapest, Hungary*
[c] *RCAES, Geodetic and Geophysical Institute of Hungarian Academy of Sciences, Hungary*
[d] *Volcano Research Group, Department of Mineralogy, Geochemistry and Petrology, University of Szeged, Szeged, Hungary*
[e] *Institute of Geodynamics, Romanian Academy, 19–21. str. Jean-Luis Calderon, 020032 Bucharest, Romania*
[f] *National Research Institute of Astronomy and Geophysics (NRIAG), Cairo, Egypt*

- Combined use of petrologic and magnetotelluric data to constrain the magma storage
- The amphibole barometry indicates that the magma chamber could have been at 8–13 km depth.
- The long lasting crystal mush was reheated by intruding basaltic magmas prior to the volcanic eruptions.
- The magnetotelluric data imply a mushy magmatic body with 5–15% melt fraction beneath the Ciomadul.
- Suggestion a term as 'volcano with potentially active magma storage' or PAMS volcano

http://dx.doi.org/10.1016/j.jvolgeores.2014.12.006
0377-0273/© 2014 Published by Elsevier B.V.

Journal of Volcanology and Geothermal Research xxx (2014) xxx–xxx

Contents lists available at ScienceDirect

Journal of Volcanology and Geothermal Research

journal homepage: www.elsevier.com/locate/jvolgeores

Combined magnetotelluric and petrologic constrains for the nature of the magma storage system beneath the Late Pleistocene Ciomadul volcano (SE Carpathians)

S. Harangi [a,b,*], A. Novák [c], B. Kiss [a,d], I. Seghedi [e], R. Lukács [a,d], L. Szarka [c], V. Wesztergom [c], M. Metwaly [f], K. Gribovszki [c]

[a] MTA-ELTE Volcanology Research Group, H-1117 Budapest, Pázmány sétány 1/C, Budapest, Hungary
[b] Department of Petrology and Geochemistry, Eötvös University, Budapest, Hungary
[c] RCAES, Geodetic and Geophysical Institute of Hungarian Academy of Sciences, Hungary
[d] Volcano Research Group, Department of Mineralogy, Geochemistry and Petrology, University of Szeged, Szeged, Hungary
[e] Institute of Geodynamics, Romanian Academy, 19–21. str. Jean-Luis Calderon, 020032 Bucharest, Romania
[f] National Research Institute of Astronomy and Geophysics (NRIAG), Cairo, Egypt

ARTICLE INFO

Article history:
Received 22 June 2014
Accepted 9 December 2014
Available online xxxx

Keywords:
Magnetotelluric
Petrology
Thermobarometry
Volcano
Magma reservoir
Ciomadul
Potentially active magma storage

ABSTRACT

The Ciomadul is the youngest volcano of the Carpathian–Pannonian region, which erupted last time at 32 ka. It produced high-K dacitic lava domes and pumiceous pyroclastic rocks. The dacite is crystal-rich and contains plagioclase, amphibole in addition to biotite, titanite, apatite, zircon and occasionally quartz, K-feldspar as well as olivine, clinopyroxene and orthopyroxene. There are two groups of amphiboles, characterized by low-Al and high-Al, respectively. They occur in the same samples and also as different zones of the same crystals. Thermobarometric calculations suggest that the low-Al amphiboles were formed from a low temperature (<800 °C) silicic magma, whereas the high-Al amphiboles crystallized at about 950 °C from a more mafic melt. A near-solidus silicic crystal mush body was stored at 7–14 km depth, where an eruptible magma batch was produced by major reheating (about 200 °C temperature increase) due to the intrusion of hot mafic magma into the silicic magma reservoir. A magnetotelluric survey was performed to reveal whether any melt-bearing magma body could presently reside beneath the volcano. Both the 2D and 3D inversion modeling calculations indicate low electric resistivity values in the depth interval of 5–25 km, just beneath the volcanic centers. This can be interpreted as implying a partially melted zone, i.e. a crystal mush body containing about 5–15% melt fraction. In addition, the 2D modeling calculation indicates also a deeper low resistivity anomaly at 30–40 km depth. The consistent petrologic and magnetotelluric constrains on the magma storage beneath Ciomadul corroborated also the recent seismic tomography result, which pointed out a low-velocity anomaly at 8–20 km depth zone. Thus, results of independent models suggest the presence of a melt-bearing crystal mush body beneath the seemingly inactive volcano. Since there are implications for long repose periods during the lifetime of the volcano as well as for effective and rapid remobilization of the low-temperature silicic crystal mush body prior to volcanic eruptions, the present existence of a low melt fraction silicic crystal mush beneath Ciomadul could mean that there is still a potential for a rejuvenation in the future. We suggest for long-dormant or seemingly inactive volcanoes, such as Ciomadul, having melt-bearing magmatic body at depths to term as 'volcano with potentially active magma storage' or PAMS volcano.

1. Introduction

There are approximately 1500 potentially active volcanoes in the Earth (Siebert et al., 2011). By definition, they include all the volcanoes that erupted at least once for the past 10 ka and there is still a chance for another eruption in the future. However, the caveat of this classification is that volcanoes can be in dormant stage even for several 10s ka (e.g., Mt. St. Helens, Clynne et al., 2008; Lassen Volcanic Center: Clynne and Muffler, 2010; Santa Maria: Escobar-Wolf et al., 2010; Volcán Tepetiltic Frey et al., 2013). Furthermore, there are evidences that mushy magma body in crustal depth could exist for more than 100 ka before volcanic eruption (Bachmann et al., 2007; Claiborne et al., 2010; Cooper and Kent, 2014). Thus, the state of a volcano can be evaluated only by integrating the eruptive history of the volcano with the information about the nature of the magma chamber beneath it. Until crystal mush body with some melt fraction is present beneath a

* Corresponding author at: MTA-ELTE Volcanology Research Group, H-1117 Budapest, Pázmány sétány 1/C, Budapest, Hungary. Tel.: +36 1372 2500x8355; fax: +36 1381 2108.
E-mail address: szabolcs.harangi@geology.elte.hu (S. Harangi).

http://dx.doi.org/10.1016/j.jvolgeores.2014.12.006
0377-0273/© 2014 Published by Elsevier B.V.

volcano, there is a potential chance for reawakening by reactivation of the locked crystal mush. There are several mechanisms to achieve crystal mush remobilization such as gas sparging from an underlying recharged magma (Bachmann and Bergantz, 2006), wholesale convection and overturn of the mush by a hot recharge (Burgisser and Bergantz, 2011) or thermomechanical unlocking by combination of remelting and erosive microfracturation (Huber et al., 2011). When the magma chamber is already solidified, there is much less chance for further eruptions due to the requirement of much more thermal energy. In summary, detection of melt-bearing magmatic body beneath dormant or even seemingly inactive volcanoes is important to characterize the state of the volcano and evaluate its possible future behavior.

Magnetotelluric method is a powerful tool to detect partial melt or fluids in the crust by quantifying the electric conductivity behavior (Newman et al., 1985; Ingham, 1988, 2005; Matsushima et al., 2001; Brasse et al., 2002; Baba et al., 2006; Schilling et al., 2006; Heise et al., 2007; Wannamaker et al., 2008; Hill et al., 2009; Ingham et al., 2009; Pommier et al., 2010b; Ádám and Szarka, 2011; Díaz et al., 2012; Spichak, 2012; Desissa et al., 2013; Park and Ostos, 2013). However, rock porosity, fluid content and the temperature at the larger depth also influence the electrical resistivity. Distinguishing whether the conductivity anomalies indicate partial melt or fluid is critical, although it is not an easy task in many cases. Laboratory impedance measurements under various pressure and temperature values conducted by Pommier et al. (2008, 2010a, 2010b) suggest that circulating mineralized water in crustal rocks could be characterized by much higher conductivity (>1000 Sm^{-1}) than silicate melts (usually 0.01–10 Sm^{-1}). Another approach could be the combined use of geophysical (magnetotelluric and seismic interpretations) and petrologic (geothermobarometric constrains on the depth and nature of the magma chamber) methods (Pommier et al., 2010b). The perspective of the magnetotelluric studies was underlined by Umeda et al. (2006) who indicated a crustal magma storage beneath the Iide Mts, Japan that was previously considered as a non-volcanic region.

The Ciomadul is the youngest volcano in the Carpathian–Pannonian region (Fig. 1; Szakács et al., 1993, 2002; Karátson et al., 2013), where the last eruption occurred at 32 ka, as given by radiocarbon measurements on charcoals found in pyroclastic deposits (Moriya et al., 1996; Vinkler et al., 2007; Harangi et al., 2010). Although the long quiescence period since the last eruption seems to imply that this volcano is already inactive, there are several indications that a hot magmatic body could still reside beneath the volcano. There is a high heat flow (85–120 mW/m^2; Rădulescu et al., 1981; Demetrescu and Andreescu, 1994) around Ciomadul, and up to 78 °C temperature was measured in a drillhole at 1140 m in Băile Tuşnad, at the western edge of Ciomadul (Rădulescu et al., 1981), there are strong CO_2 emanations often accompanied with release of H_2S and SO_2 and the $^3He/^4He$ isotope ratio of natural gases and CO_2-rich mineral waters implies magmatic origin (Althaus et al., 2000; Vaselli et al., 2002). Furthermore, a recent seismic investigation pointed out a low-velocity anomaly just beneath the volcano with a possible magma reservoir between 8 and 20 km depths (Popa et al., 2012). Thus, Szakács et al. (2002), Harangi (2007) and Szakács and Seghedi (2013) emphasized that Ciomadul should be regarded as a potentially active volcano, where rejuvenation of volcanism cannot be unambiguously excluded. Here we provide the result of a magnetotelluric survey across the volcanic edifice combined with the data of the geobarometric calculations using amphiboles and plagioclases of the dacites (Kiss et al., 2014) to test the feasibility whether the detected parameters could be linked to a potential melt presence in crustal depth beneath the volcano.

2. Geological background

The Ciomadul volcano is located at the southern termination of the Călimani–Gurghiu–Harghita (CGH) andesitic–dacitic volcanic chain, at the southeastern edge of the Carpathian–Pannonian region (Fig. 1; Szakács et al., 1993; Szakács and Seghedi, 1995). The volcanism along the CGH is characterized by a gradually younging volcanism from 11.3 Ma (Peltz et al., 1987; Pécskay et al., 1995). There was a sharp compositional change of the erupted magmas within the Harghita Mountains around 3 Ma and since that time more potassic and incompatible element-enriched volcanic products have been formed (Seghedi et al., 1987; Szakács et al., 1993; Mason et al., 1996). Termination of the volcanic activity at the southern Harghita was followed by eruption of even more potassic magmas after a couple of 100s ka repose time. Shoshonitic magmas with strongly mixed mineralogical character formed isolated cryptodome bodies at about 1.5 Ma (e.g., Mason et al., 1995; Pécskay et al., 1995; Mason et al., 1996). The age of the volcanism in the Ciomadul is controversial. K/Ar dating indicates that the volcanic activity could commence at 500–600 ka after sporadic lava dome effusions at about 900–1000 ka (Pécskay et al., 1992, 1995). However, according to the (U–Th)/He zircon ages Ciomadul could be much younger (<200 ka; Karátson et al., 2013). The volcanism of the Ciomadul is characterized by an initial lava–dome complex development, whereas in the latest phase, vulcanian to sub-plinian explosive eruptions were more frequent. As a result, two explosion craters were formed, the Mohos and the Sf. Ana craters (Szakács and Seghedi, 1995). The former one is covered presently by a swamp, whereas the youngest crater is filled by a lake (Magyari et al., 2009, 2014). The erupted magma remained fairly homogeneous through Q7 time and shows high-K dacitic composition (Szakács and Seghedi, 1986; Vinkler et al., 2007).

The geodynamic setting of the CGH volcanism and particularly the volcanic activity of southern Harghita and Ciomadul is still debated. Gradual slab-break off of the subducted slab, lithospheric delamination either following the subduction or due to gravitational instability was invoked to explain the tectonic evolution of this region (e.g. Gîrbacea and Frisch, 1998; Mason et al., 1998; Chalot-Prat and Gîrbacea, 2000; Sperner et al., 2001; Lorinczi and Houseman, 2009; Fillerup et al., 2010; Koulakov et al., 2010; Seghedi et al., 2011; Ren et al., 2012). Nevertheless, an active geodynamic situation is clearly indicated by the continuous seismicity attributed to the descent of a near vertical slab beneath the Vrancea zone (Oncescu et al., 1984; Sperner et al., 2001; Popa et al., 2012) about 50 km southeast from Ciomadul. This exhibits the largest present-day strain concentration in continental Europe (Wenzel et al., 1999).

3. Analytical conditions

3.1. Petrologic investigations

Fresh samples were collected both from lava dome rocks and from pumiceous pyroclastic deposits. Composition of the mineral phases of the Ciomadul dacites was determined using a CAMECA SX100 electron microprobe equipped with four WDS and one EDS at the University of Vienna, Department of Lithospheric Research (Austria). The operating conditions were as follows: 15 kV accelerating voltage, 20 nA beam current, 20 s counting time on peak position and PAP correction procedure for data reduction. Amphibole and plagioclase crystals were measured with defocused beam (3–5 μm). Calibration was based on the following standards: Amelia albite (Na, Si, Al), San Carlos olivine (Mg), almandine 112140 (Fe), microcline (K), wollastonite (Ca), rutile (Ti) and spessartine (Mn).

3.2. Magnetotelluric survey and data quality

Magnetotellurics (MT) is a geophysical technique characterizing the electric conductivity (or its reciprocal quantity, the electrical resistivity) structure at depth, applying a very large natural electromagnetic (EM) source of magnetosphere origin. The time variations of the EM field penetrate into the subsurface, where they are attenuated, depending on the period length of the variations. At the surface, the magnetotelluric transfer function (the MT impedance, i.e. the complex relationship between

Please cite this article as: Harangi, S., et al., Combined magnetotelluric and petrologic constrains for the nature of the magma storage system beneath the Late Pleistocene Ciomadu..., J. Volcanol. Geotherm. Res. (2014), http://dx.doi.org/10.1016/j.jvolgeores.2014.12.006

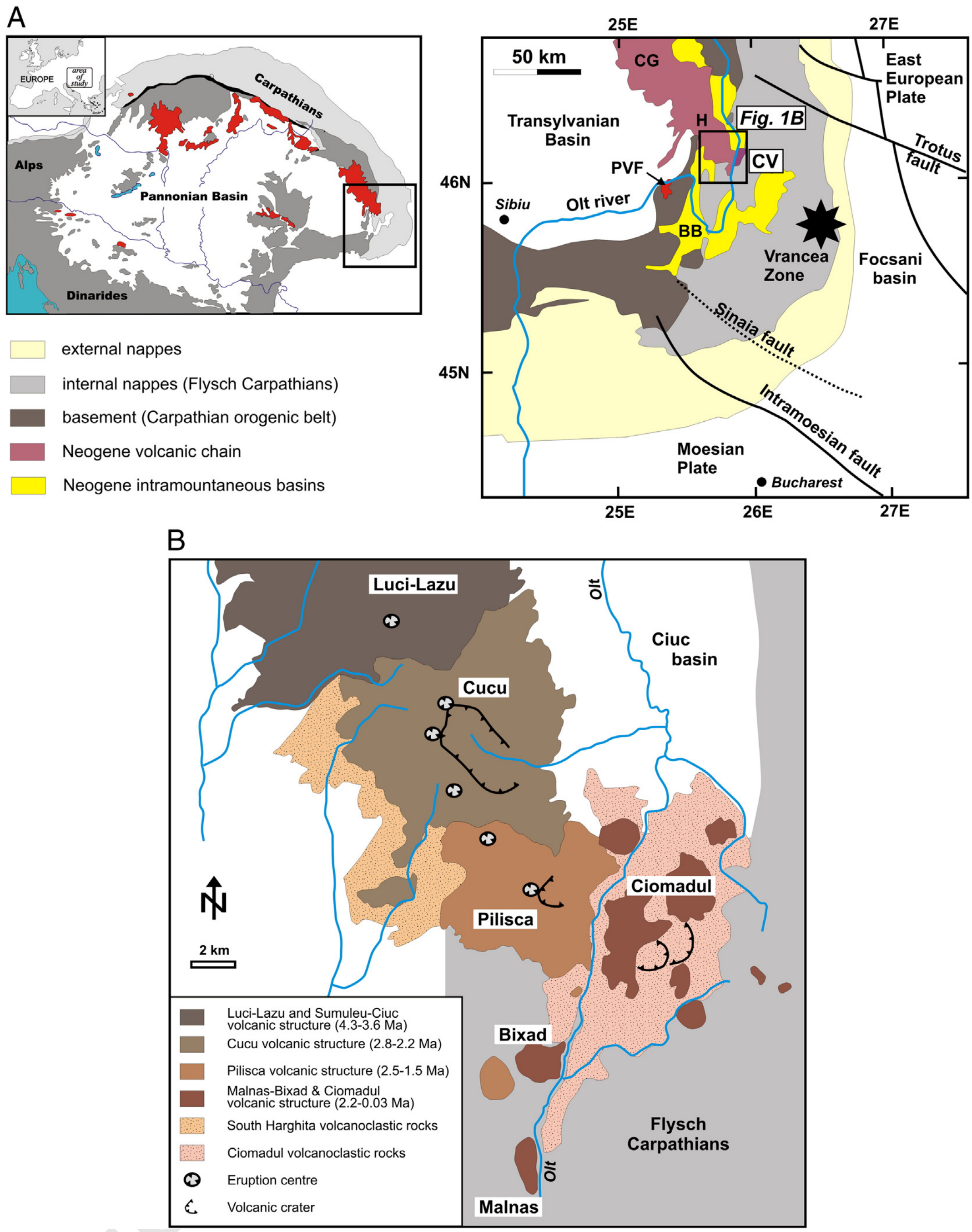

Fig. 1. A. Location of the Ciomadul volcano (CV) in the southeastern Carpathian area of the Carpathian–Pannonian Region (red colors denote the Miocene to Pliocene andesite–dacite volcanoes). CG = Călimani–Gurghiu volcanic complex, H = Harghita volcanic complex, BB = Braşov basin, PV = Perşani basalt volcanic field. Geological map is after Cloetingh et al. (2004) and Martin et al. (2006). B. Simplified geological map of the South Harghita–Ciomadul volcanic area modified after Seghedi et al. (1987). The South Harghita volcanic field comprises the Luci-Lazu, Cucu and Pilisca volcanic complexes. The Malnas and Bixad are two shoshonitic cryptodomes. The Ciuc basin is a Pliocene–Quaternary intramontane basin. The Ciomadul volcanic complex is underlain by Cretaceous Flysch sedimentary formations. (For interpretation of the references to color in this figure legend, the reader is referred to the web version of this article.)

the recorded electric and magnetic field variations) depends on the electrical resistivity structure beneath the surface. The MT method is able to reveal if there is any melt-bearing magmatic body at depth below the given field site.

In autumn 2010 we carried out twelve long period magnetotelluric soundings in the investigated area (Fig. 2). The time variations of the magnetic field components (Hx, Hy and Hz) were measured by using induction coils, while the Ex, Ey electric ("telluric") field components were measured by using 50 m long electric dipoles. The average distance among the 12 field stations varied between 1 km and 4 km. Due to the 4–5 days long continuous recording of the EM fields at each station, it was possible to observe time variations in the period range of 0.25–15,000 s. A simultaneous use of three different LEMI 417 acquisition systems, allows applying remote and cross reference techniques, which is an efficient technique to eliminate EM noise of artificial origin.

Due to surface roughness, hillside location, and various technical difficulties, the spacing between the neighboring MT stations could not be equidistant. At a part of the field stations (usually close to inhabited areas and/or to railway lines), strong artificial electromagnetic noise was observed. At some sites the telluric wires were occasionally bitten and cut by wild animals. Due to the fact that the effective recording time sufficient to estimate the MT transfer function for the investigated

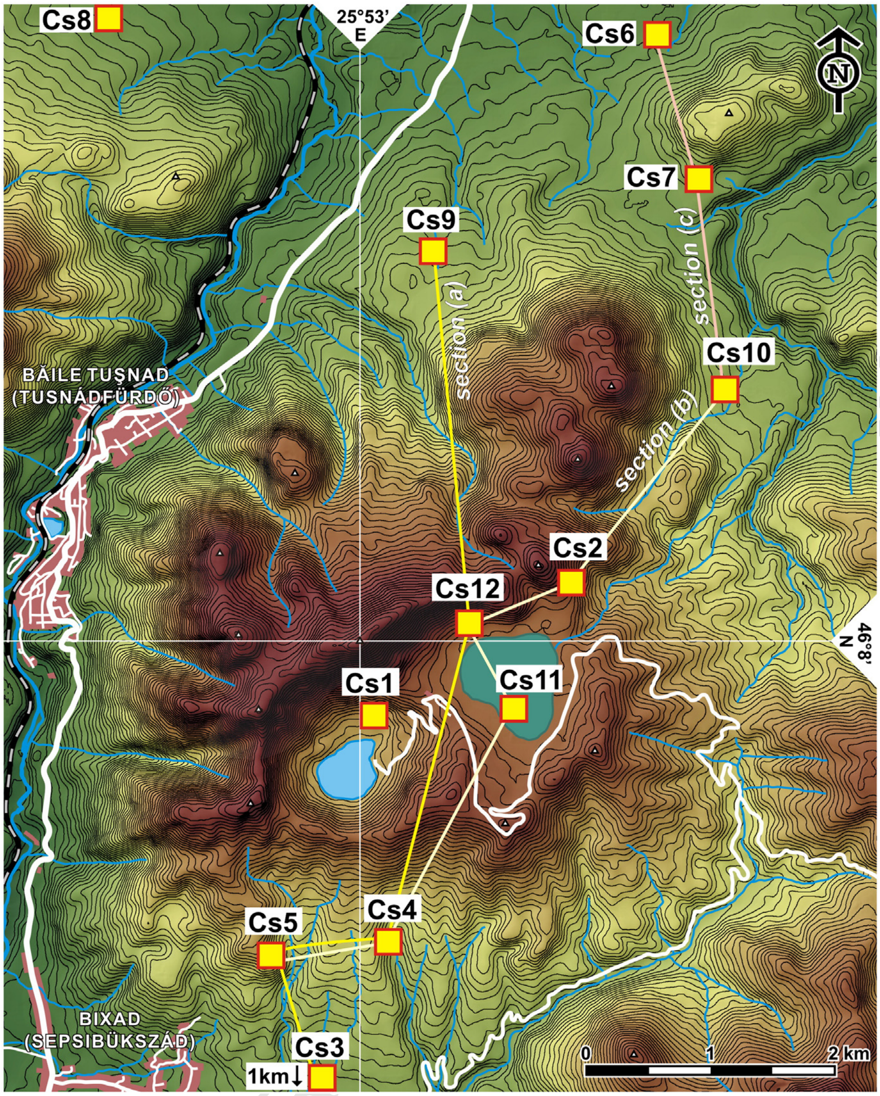

Fig. 2. Location of the MT stations in Ciomadul and the sections used to construct the 2D modeling profiles in Fig. 8. Topographic map after Karátson et al. (2013).

depth range is about 1–2 days, and our record length was 2–5 times longer (4–5 days/station), the aforementioned disturbances and damages did not make impossible to construct full MT sounding curves. The natural electromagnetic variation (i.e. variation of solar wind origin) was relatively low in autumn 2010, when the MT soundings were carried out. The data were processed by using robust single-site processing code, and, in some cases, remote reference processing code, in order to eliminate artificial electromagnetic noises and to estimate MT transfer functions with different approaches (Verő, 1972; Egbert and Booker, 1986; Egbert and Livelybrooks, 1996).

4. Results

4.1. Petrology of the Ciomadul dacite

The Ciomadul lava dome rocks and pumices are relatively homogeneous in composition ($SiO_2 = 62–68$ wt.%, $K_2O = 3.0–3.6$ wt.%, $Na_2O = 4.0–4.6$ wt.%; Szakács and Seghedi, 1986; Mason et al., 1996; Vinkler et al., 2007) and are calc-alkaline, high-K dacites. The crystal content is relatively high in the lava dome rocks (30–40 vol.%), whereas pumices contain less phenocrysts (10–15 vol.%). The crystal assemblage is fairly diverse; in addition to the dominant plagioclase, amphibole and biotite phenocrysts (Fig. 3A), titanite, apatite, zircon are commonly observed, occasionally with quartz, K-feldspar, allanite and clinopyroxene, olivine and orthopyroxene. This complex mineral assemblage implies mixing of silicic and mafic magmas prior to the eruptions (Kiss et al., 2014). A notable feature of many dacite samples is the occurrence of felsic crystal clots (Fig. 3B), which contain the same mineral population as the host rock. They often consist of 10–15 vol.% interstitial vesiculated glass. Clinopyroxene and olivine form crystal clots with minor plagioclases, but they occur also solely in the silicic groundmass.

Plagioclase is the most abundant mineral phase occurring either in large glomerocrystic aggregates or as euhedral microphenocrysts. The An-content is in the range from 25 to 60 mol% in both plagioclase types, but they differ in FeO content. The glomerocrystic plagioclases are characterized by typically low FeO ($FeO < 0.2$ wt.%) while the FeO content of the microphenocrysts shows large variation with up to 0.55 wt.% values. It is remarkable that the outermost rim of the glomerocrystic plagioclases in the older lava dome rocks has often elevated FeO akin to that of the microphenocrystic plagioclases. They contain mineral inclusions such as amphibole and occasionally titanite and zircon. Amphiboles occur in diverse textural forms (Fig. 3B) and show a wide compositional range ($Al_2O_3 = 6–15$ wt.%, $MgO = 10–18$ wt.%; Table 1., Fig. 4A) even within single samples (Kiss et al., 2014). They can be classified into two groups, a low-Al and a high-Al ones that are common in many intermediate arc volcanoes (e.g., Redoubt, Coombs et al., 2013; Unzen, Sato et al., 2005; Soufriére Hills, Murphy et al., 2000; Mt. Pelée, Pichavant et al., 2002; Pinatubo, Pallister et al., 1996).

Please cite this article as: Harangi, S., et al., Combined magnetotelluric and petrologic constrains for the nature of the magma storage system beneath the Late Pleistocene Ciomadu..., J. Volcanol. Geotherm. Res. (2014), http://dx.doi.org/10.1016/j.jvolgeores.2014.12.006

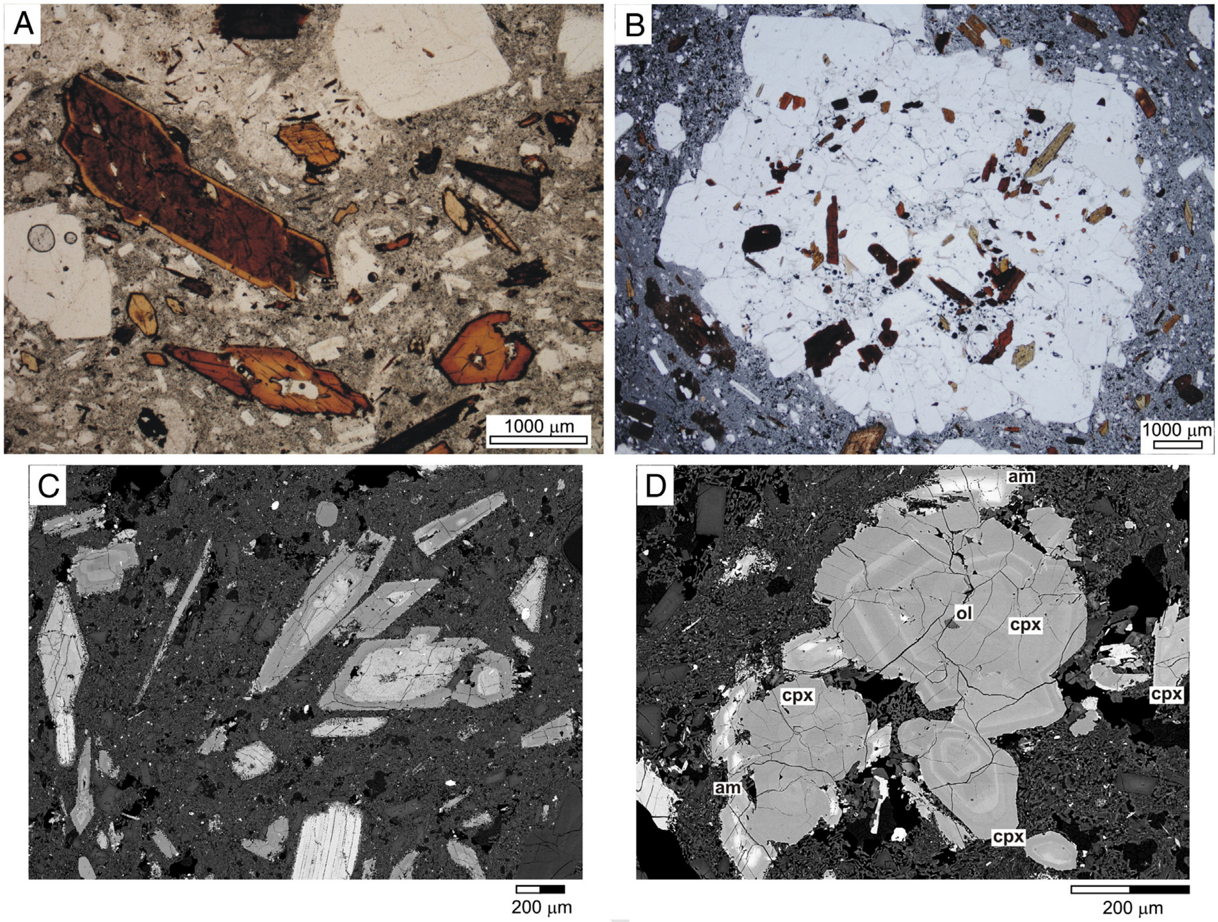

Fig. 3. Representative microscopic images of the Ciomadul dacite: A. Characteristic occurrences of amphibole and plagioclase phenocrysts and microphenocrysts in the lava dome rocks (optical microscopic picture with one nicol); B. Felsic inclusions (crystal clots) are common in a dacite. They have cumulate texture, but with some interstitial glass and are composed of plagioclases, amphibole, titanite, apatite, biotite and zircon (optical microscopic picture with one nicol). C. Back scattered image of a lava dome rocks. Note the different zoning patterns and reaction rims of the amphibole phenocrysts. They can be subdivided into two groups: hornblendes (low-Al amphibole) with thicker reaction rim and pargasites (high-Al amphibole) with stronger zoning and very thin reaction rim. D. Clinopyroxene crystal clot in dacitic lava dome rock. In the back-scattered image oscillatory zoning of the clinopyroxene crystals can be clearly observed. cpx = clinopyroxene; ol = olivine; am = amphibole.

The low-Al amphiboles are in close coexistence with the low-FeO plagioclases, quartz, biotite, titanite and K-feldspar, whereas the high-Al amphiboles can occur with the plagioclase microphenocrysts and as overgrowths on olivine and clinopyroxenes. Majority of olivines, orthopyroxenes and clinopyroxenes is characterized by high MgO content (Fo = 84–90 mol% and mg-number = 0.85–0.91, respectively) that implies derivation from primitive basaltic magma. The high-Mg olivines are surrounded by thick reaction corona, however, in rare cases they have unresorbed margin similarly as some high-Mg clinoproxenes. While the olivines are mostly slightly zoned, clinopyroxenes often show oscillatory and reverse zoning with fluctuation of the mg-number along with the Cr-content (Table 2, Fig. 3D). Magnesian orthopyroxenes occur

Table 1
Representative major element composition of Ciomadul amphiboles and the calculated crystallization temperature and pressure.

Sample	TC15	Kp9-30b	KCS17-100	Tf13-1	KCS17-100	BX08/1	BX28-3-sza	TC15
	Low-Al				*High-Al*			
Crystal	am4	am3	amf_sz_2am	am2 no.2	am2	am9	amf_9_c	am6
	Felsic crystal clot	Felsic crystal clot						
SiO_2	44.98	44.91	43.93	47.17	44.14	44.05	44.45	44.89
TiO_2	1.32	1.25	1.27	0.96	2.20	1.58	1.39	1.94
Al_2O_3	8.57	8.28	8.49	7.28	11.61	10.41	11.33	10.97
FeO[a]	15.33	15.51	15.76	14.24	8.18	12.18	7.72	7.62
MgO	12.19	11.83	12.41	13.41	16.09	13.99	17.01	16.74
MnO	0.42	0.44	0.4	0.44	0.12	0.20	0.08	0.12
CaO	11.86	11.72	11.73	11.70	11.75	11.77	11.70	11.93
Na_2O	1.48	1.53	1.44	1.40	2.24	2.04	2.40	2.07
K_2O	0.94	0.90	0.97	0.72	0.90	0.83	0.88	0.81
Total	97.09	96.36	97.04	97.31	97.229	97.11	97.03	96.10
T °C	728	704	756	705	956	893	950	941
P MPa	347	365	295	270	325	207	301	276

[a] All Fe as FeO.

Please cite this article as: Harangi, S., et al., Combined magnetotelluric and petrologic constrains for the nature of the magma storage system beneath the Late Pleistocene Ciomadu..., J. Volcanol. Geotherm. Res. (2014), http://dx.doi.org/10.1016/j.jvolgeores.2014.12.006

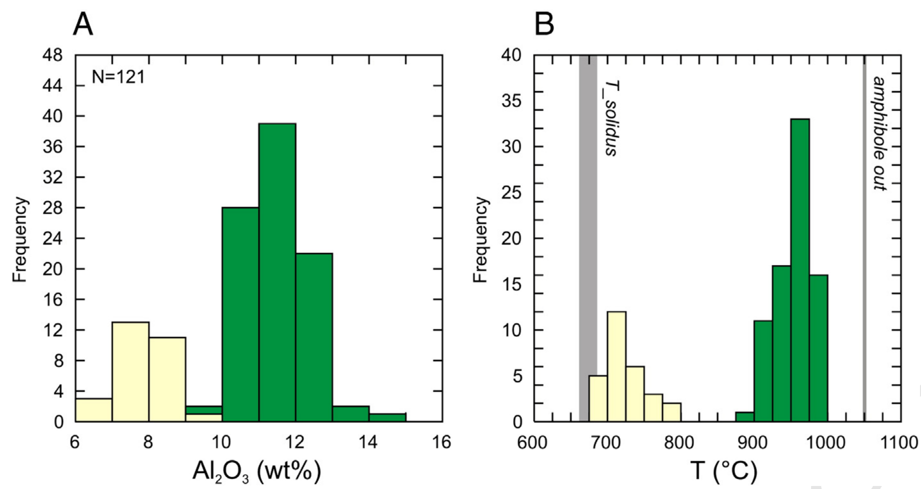

Fig. 4. A. Variation of the Al_2O_3 content (in wt.%) of the Ciomadul dacites. yellow color denotes the low-Al amphiboles, whereas green indicates high-Al amphiboles; B. Distribution of the calculated crystallization temperature (in °C) of the amphiboles based on the thermometer of Anderson et al. (2008) for low-Al amphiboles and Ridolfi et al. (2010) and Ridolfi and Renzulli (2012) for high-Al amphiboles. The thick gray line indicates the water saturated solidus temperature (T_solidus) of dacite at 200–300 MPa according to Holtz et al. (2001). The thin gray line is the maximal stability temperature in °C for amphiboles at 200–300 MPa based on the experimental results of Barclay and Carmichael (2004) and Adam et al. (2007). (For interpretation of the references to color in this figure legend, the reader is referred to the web version of this article.)

mostly in the pumices and they are surrounded by well-developed reaction rim bracketed by amphibole.

5. Thermobarometric calculations

Occurrence of amphiboles and their coexistence with wide range of minerals enable to perform thermobarometric calculations to constrain the condition of the crystallization (e.g., Hammarstrom and Zen, 1986; Johnson and Rutherford, 1989; Blundy and Holland, 1990; Anderson and Smith, 1995; Bachmann and Dungan, 2002; Ridolfi et al., 2010). Composition of amphiboles is particularly sensitive on pressure (Johnson and Rutherford, 1989; Schmidt, 1992; Anderson and Smith, 1995; Anderson et al., 2008), and thus, it is widely used to estimate the depth of crystallization (converting pressure to depth, we assume 2.85 g/cm^3 average density of the crustal rocks). The single amphibole geobarometers of Ridolfi et al. (2010) and Ridolfi and Renzulli (2012) are commonly applied to constrain the depth of magma chambers beneath intermediate arc volcanoes (e.g., Scott et al., 2012; Chambefort et al., 2013; Costa et al., 2013; Turner et al., 2013; Walker et al., 2013). In this case, amphiboles with wide compositional range could imply either a vertically extended magma reservoir or separated magma chambers at different depths. Results of these geobarometers were recently tested using compositionally zoned amphiboles and experimental data and it turned out that the large calculated pressure variation provided by the Ridolfi et al. (2010) or Ridolfi and Renzulli (2012) geobarometers is only apparent and reflects crystallization of amphiboles at different temperature and/or from different magmas (Shane and Smith, 2013; Erdmann et al., 2014; Kiss et al., 2014). The pressure estimates obtained for bimodal amphibole populations in arc magmas can be explained rather by crystallization in cold, felsic magmas and hot, mafic magmas, respectively than by formation in two reservoirs at different depths (Erdmann et al., 2014; Kiss et al., 2014). Thus, a careful textural and compositional investigation, involving a comparison of the amphibole compositions with experimental data and considering their coexisting mineral assemblage, is necessary before conducting the thermobarometric calculations.

We estimated the crystallization temperature of the low-Al amphiboles using the calculation scheme developed by Anderson et al. (2008), whereas for the high-Al amphiboles we used the thermometric calibrations of Ridolfi et al. (2010) and Ridolfi and Renzulli (2012), which provided more reliable temperature values (Kiss et al., 2014). We obtained less than 800 °C with an average of 740 °C (Fig. 4B) crystallization temperature for the low-Al amphiboles. This is consistent with the experimental results on dacitic rocks containing similar coexistent mineral assemblage (e.g., Fish Canyon tuff; Johnson and Rutherford, 1989) and the occurrence of zircons with high Hf content (>11,000 ppm; Claiborne et al, 2010) in the Ciomadul dacite. In contrast, compositional features of the high-Al amphiboles resemble those crystallized above 900 °C in the experiments (Kiss et al., 2014). Indeed, we got temperature values between 900 °C and 1000 °C with an average of 950 °C (Fig. 4B).

The composition, the low crystallization temperature and the coexisting mineral assemblage (quartz + plagioclase + K-feldspar + biotite + titanite) of the low-Al amphiboles allow the use of the Al-in-amphibole barometer introduced first by Hammarstrom and Zen (1986). This barometer was further developed later (e.g., Schmidt, 1992; Anderson and Smith, 1995) and we used the temperature dependent calculation scheme of Anderson et al. (2008). We obtained crystallization pressure for the low-Al amphiboles ranged between 200 and 365 MPa with a mean value of 285 ± 45 MPa. That corresponds to a crystallization depth of 7–14 km. For the high-Al amphiboles, we got an overlapping pressure range with the previous results, but with a shift toward greater pressure values (200–500 MPa with an average 324 ± 62 MPa) using the Ridolfi et al. (2010) geobarometer.

Table 2
Representative major element composition of Ciomadul clinopyroxenes (core and rim analyses). mg-number = Mg^{2+} / (Mg^{2+} + Fe^{tot}).

Sample	KCs17 cpx3		Mo2 cpx5		Mo2 cpx7	
	Core	Rim	Core	Rim	Core	Rim
SiO_2	52.70	53.30	52.91	51.20	52.07	52.62
TiO_2	0.42	0.20	0.33	0.72	0.35	0.40
Al_2O_3	1.80	1.13	1.96	3.65	2.31	2.17
Cr_2O_3	0.12	0.30	0.31	0.04	0.01	0.19
FeO	4.15	3.66	3.25	5.21	5.47	3.63
MnO	0.12	0.13	0.08	0.13	0.22	0.10
MgO	18.81	19.49	17.75	16.33	16.20	17.46
CaO	21.14	20.62	23.12	22.28	22.72	22.98
Na_2O	0.24	0.19	0.27	0.34	0.40	0.29
Total	99.50	99.03	100.00	99.89	99.76	99.84
mg-num	0.89	0.90	0.91	0.85	0.84	0.90

6. Magnetotelluric results: strike direction, induction arrows and dimensional analyses

Several characteristic MT sounding curves with apparent electric resistivity and impedance phase values are shown in Fig. 5. Unfortunately it was site Cs1, close to the Sf. Ana Lake, i.e. inside the main explosion crater, where the MT sounding curves were of the poorest quality, so this field station had to be excluded from the interpretation. At first, prior to the inversion and modeling process, we checked the magnetotelluric strike direction from the data. Estimations were made by using three standard approaches: the "impedance strike" (Swift angle — Swift, 1967), the "tipper strike", and the "phase sensitive skew" (Bahr, 1988, 1991). The rose diagrams obtained from the tipper strike angles are shown in Fig. 6. The strike is around N30°E, where at longer periods it has a complex feature. The impedance strike was very complex; phase sensitive strike indicates again a strike direction of about N30°E. Therefore, for some further magnetotelluric modeling, a general strike direction of N30°E can be assumed. The so-called induction arrows, which are calculated from the tipper (i.e. the ratio of vertical to horizontal magnetic field) provide an additional indicator. The induction arrows in Fig. 7 are plotted according to the Parkinson convention (the "reverse" Wiese convection, Wiese, 1962), where their real parts point to the high conductivity (low resistivity) structures. The chaotic behavior of induction arrows at short periods is probably caused by shallow small-scale structural or lithological resistivity anomalies. At longer (approximately T = 100 s) periods the arrows are aligned to southeast direction, while toward even longer (approximately T = 1000 s) periods, they are turning to northeast. At the longest periods the coherence disappears again. In the 100 s–1000 s period range the structure may be considered as two-dimensional (2-D), except near the main volcanic crater filled by the Sf. Ana lake.

The subsurface electromagnetic structure beneath any volcano is complex, because it might consist of variably altered, clayey formations, hydrothermal fluids as well as a magma storage zone. The dimensionality analysis that we carried out (not shown in figure) confirms this complexity. Nevertheless, the magnetotelluric strike direction and the induction vectors allow applying two-dimensional (2-D) approaches.

7. Magnetotelluric data modeling and inversion

7.1. Two-dimensional inversion

We carried out 2-D model computations, by inverting MT impedances using non-linear conjugate gradient algorithm by Rodi and Mackie (2001). From the set of the MT sites we defined three different elongated profiles: (a) N–S, (b) NNE–SSW, (c) NNW–SSE (Fig. 8). Two of them (profiles (a) and (b)) cross the volcanic crater (Sf. Ana lake) and the third one (profile (c) in the NE part of the investigated area) points to NNW–SSE direction. Before defining the final models, a number of tests were carried out for searching the smoothing parameters, error floors etc. The starting model for the inversion was a homogeneous half-space with an electrical resistivity of 100 Ω m, where the surface topography was taken into account. In the inversion process we used the measured data errors (if they existed), otherwise an error

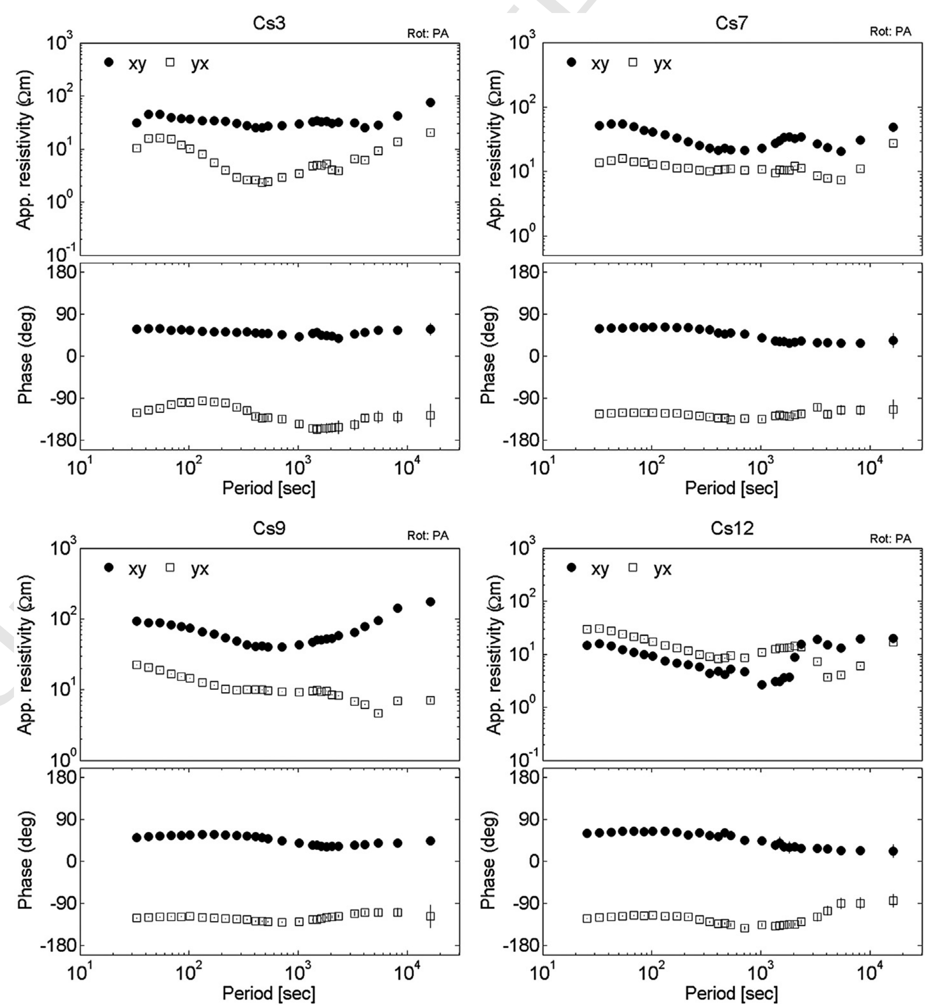

Fig. 5. MT sounding curves at four selected sites (Cs3, Cs7, Cs9, Cs12; Fig. 2).

Please cite this article as: Harangi, S., et al., Combined magnetotelluric and petrologic constrains for the nature of the magma storage system beneath the Late Pleistocene Ciomadu..., J. Volcanol. Geotherm. Res. (2014), http://dx.doi.org/10.1016/j.jvolgeores.2014.12.006

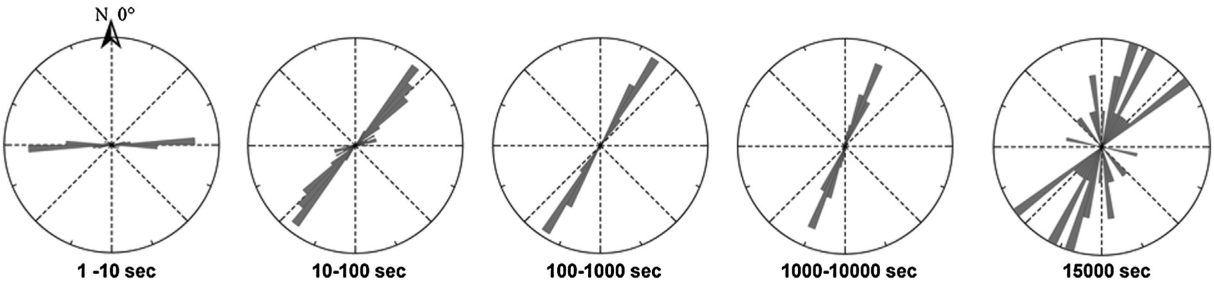

Fig. 6. Strike directions at five period ranges, calculated from the tipper values.

floor of 10% (for the apparent resistivity values) and 5% for the impedance phase values were applied. The static shift correction was automatically corrected, and the root mean square misfit (RMS) was minimized to 100 iterations. Inversions were carried out separately for both polarization modes (TE and TM), and, as a third version, a bimodal inversion (TE + TM) was also carried out. The RMS misfit along all the three profiles converged below 6%. From the inversion results the best fitting solution was selected. In profile (a), a low resistivity structure with $<5\ \Omega$ m values that correspond to 0.3–0.8 Sm^{-1} conductivity values was found in the depth range of 5–25 km (Fig. 8). The horizontal extension of this anomaly is less than 6–7 km. A similar anomaly is shown in the profile (b), and its source seems to be more or less of the same size as that in profile (a). This anomaly is located near the main volcanic crater. In profile (c) there is no any low-resistivity zone in this shallow (5–25 km deep) depth range. Instead, the low-resistivity zone appears here much deeper, in the depth range of 30–40 km (Fig. 8).

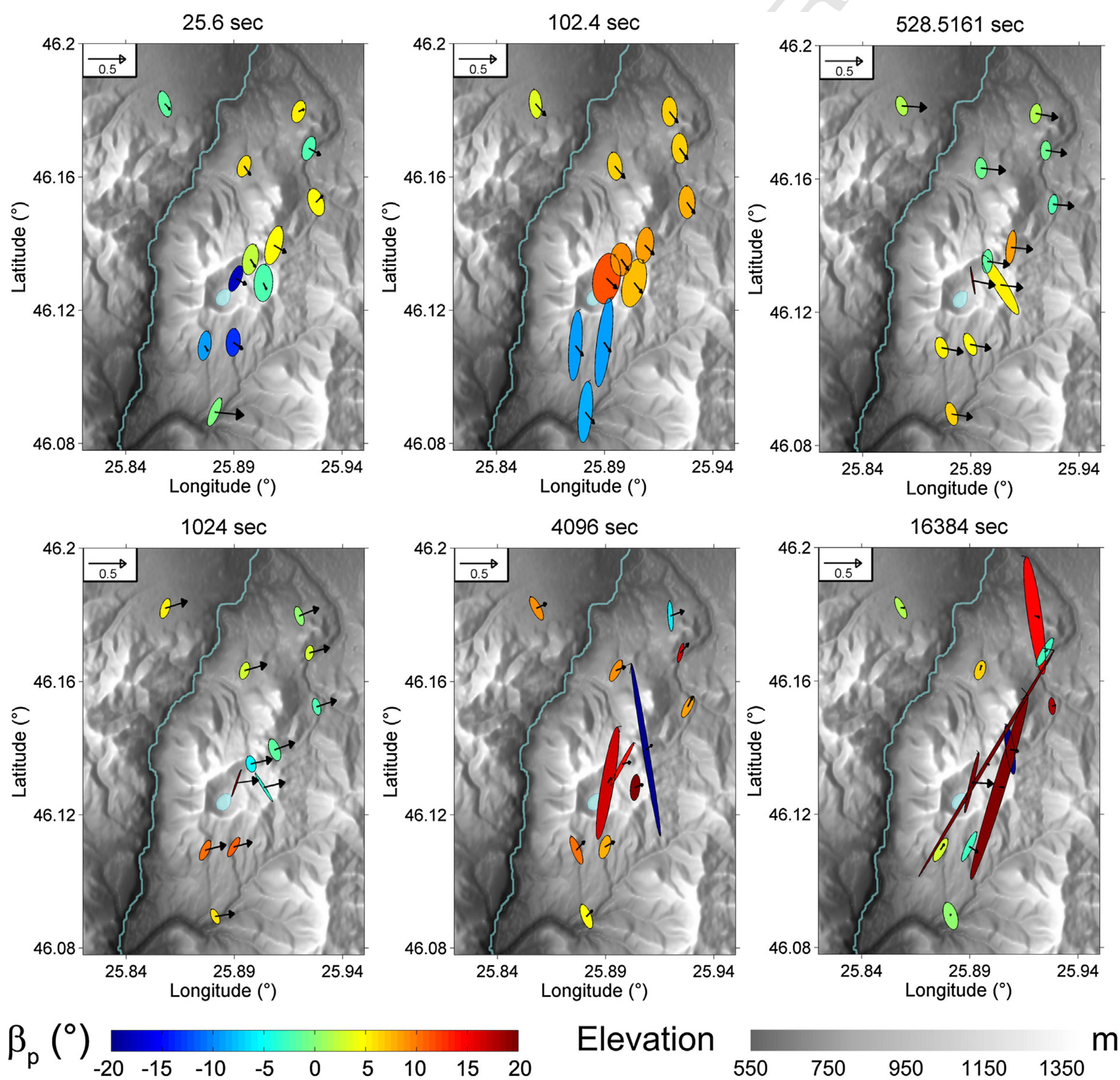

Fig. 7. The phase tensor ellipses and real induction arrows (in the so-called Wiese convection) in the horizontal map at six periods. The fill of ellipses represents the βp skew angle in degree (Wiese, 1962; Caldwell et al, 2004).

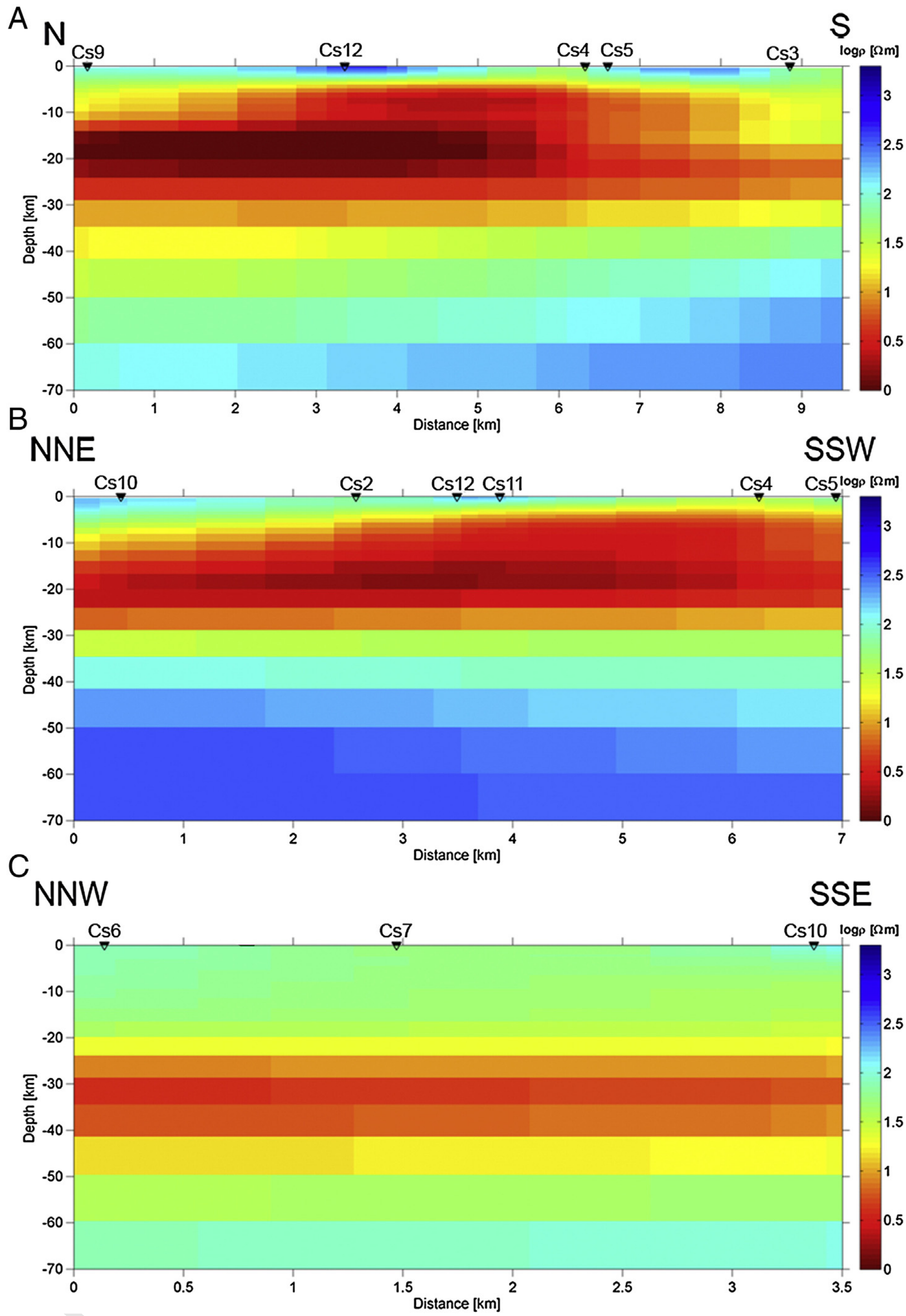

Fig. 8. 2-D inversion results along three selected profiles. Bimodal inversion with H_z conjugate was applied, based on inversion code by Rodi and Mackie (2001). Resistivity values are in logarithmic scale: a) NS profile with sites: 9-12-4-5-3 (RMS 5.6%); b) NNE–SSW profile with sites: 10-2-12-11-4-5 (RMS 2.075%); c) profile 6-7-10 (RMS 0.88%).

7.2. 3-D modeling and inversion results

We performed a 3-D inversion by using the WSIN3DMT inversion code (Siripurnvaraporn and Egbert, 2000; Siripurnvaraporn et al., 2005a, 2005b), applying 49 cells in horizontal (N–S and E–W) directions and 32 cells in vertical direction. The horizontal dimensions of the central cell in the grid were set to 10 × 10 km. The considered domain horizontally extended to 1945 km and vertically it extended to a depth of 508 km. The input data for the 3-D inversions from the 12 field stations were the values of imaginary and real parts of the impedance tensor elements Zxx, Zxy, Zyx and Zyy, determined at 13 various periods. The topography in the 3-D inversion was ignored. The inversion after 7 iterations arrived to a good fit between the measured and the modeled values, characterized by 1.92% RMS. The low resistivity anomaly in the depth range of 5–20 km, drawn from 2-D inversion, was confirmed by the 3-D inversion (Fig. 9). However, there is a significant difference between the 3-D and 2-D inversion results: in 3-D inversion, at deeper part there was no indication for a low resistivity zone. This contradiction between the 2-D and 3-D results might be resolved by the behavior of the vertical magnetic field, which was considered in the 2-D inversion, and was ignored in the 3-D one. As seen from the induction arrows and the so-called phase ellipses, at the apparent depth of 25 km, there is an evident deepening tendency from SW toward NE direction. A comparison between 3-D and 2-D inversion results are shown in Fig. 10.

Please cite this article as: Harangi, S., et al., Combined magnetotelluric and petrologic constrains for the nature of the magma storage system beneath the Late Pleistocene Ciomadu..., J. Volcanol. Geotherm. Res. (2014), http://dx.doi.org/10.1016/j.jvolgeores.2014.12.006

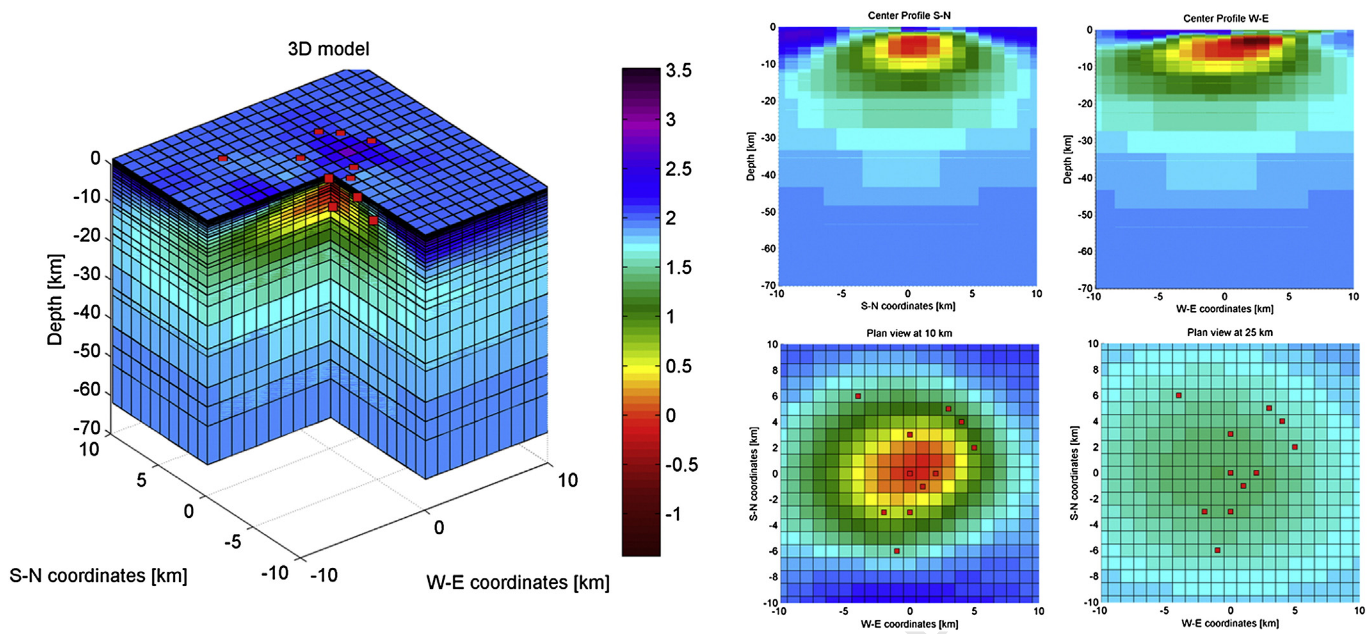

Fig. 9. 3-D model of the investigated area by 3-D inversion results in different view. Resistivity values are in logarithmic scale. The MT stations are shown by red dots. (For interpretation of the references to color in this figure legend, the reader is referred to the web version of this article.)

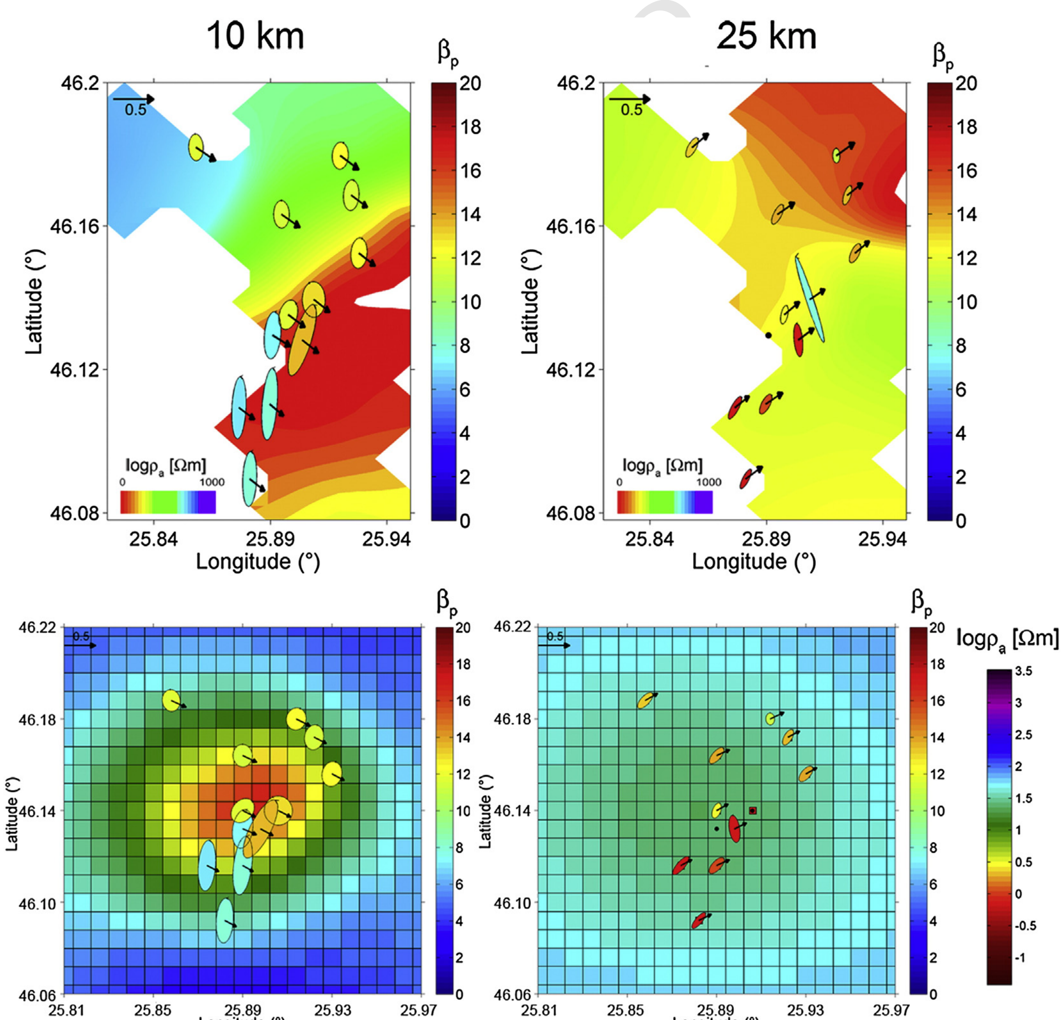

Fig. 10. Comparison of 2-D and 3-D inversion results, shown in the form of maps at apparent depths of 10 and 25 km. The fill of ellipses represents the βp skew angle in degree. Resistivity values are in logarithmic scale.

Please cite this article as: Harangi, S., et al., Combined magnetotelluric and petrologic constrains for the nature of the magma storage system beneath the Late Pleistocene Ciomadu..., J. Volcanol. Geotherm. Res. (2014), http://dx.doi.org/10.1016/j.jvolgeores.2014.12.006

8. Discussion

8.1. Petrologic constrains on the condition of the magma storage

Magmatic system beneath volcanoes is regarded to have a complex architecture and is different from the single circular, melt-bearing magma chamber view. The magma reservoir or magma storage contains interconnected crystal-melt mush zones (non-eruptible part of the magma body), occasionally with melt-dominated regions or lenses (eruptible magma), which can be termed as magma chamber (Hildreth, 2004; Annen et al., 2006; Hildreth and Wilson, 2007; Bachmann and Bergantz, 2008; Cashman and Sparks, 2013; Cooper and Kent, 2014). There could be a continuation of this shallow crustal magma reservoir toward the depth, where further magma reservoirs may exist either composed by crystal mush or are already in solid state. At the crust–mantle boundary, an extensive magma storage zone can be present, where mantle-derived mafic magmas could accumulate (Stroncik et al., 2009) or could mix with crustal melt (Hildreth, 1981), altogether forming the 'hot zone' (Annen et al., 2006). The volcano petrology is a powerful tool to characterize this complex system using integrated textural and geochemical studies combined with thermobarometric calculations (e.g., Humphreys et al., 2006; Shcherbakov et al., 2011; Viccaro et al., 2012; Kiss et al., 2014).

The Ciomadul dacites have a fairly diverse crystal assemblage that can be divided into a low-temperature (<800 °C) mineral population (low-FeO plagioclase glomerocrysts, low-Al amphibole, biotite, quartz, K-feldspar, titanite, apatite, zircon, and allanite) and a high-temperature (>900 °C) mineral group (plagioclase microphenocrysts, high-Al amphibole, olivine, clinopyroxene, orthopyroxene). The low-temperature mineral assemblage is also found as felsic crystal clots, which can be interpreted to represent fragments of a crystal mush body, having a long lifetime beneath the volcano at temperature close to the solidus of granodioritic/dacitic system (Kiss et al., 2014). This magma storage is regarded as a heterogeneous silicic magma reservoir, where crystals and melts existed with variable relative amounts, but overall, it consisted of a non-eruptible magma body (i.e., crystals ≫ melt). The compositional zoning of zircons and textural features of olivines and clinopyroxenes (not detailed here) suggest that the felsic shallow crustal magma storage was developed by intermittent pulses of silicic magma ascent and repeated intrusions of basaltic magmas. This sequence of events could keep the magma reservoir at temperature above the solidus temperature for 10s ka with no volcanic eruption. The geobarometric calculations from the low-Al amphiboles indicate that this felsic magma reservoir resided at 7–14 km depth (Fig. 11). Among the amphiboles, there are crystals with a zoning type where high-Al amphibole rim is observed around low-Al amphibole cores. This clearly suggests that both amphibole types crystallized in the same magma reservoir at similar depth and not in distinct magma storage zones (Kiss et al., 2014). Furthermore, it implies that a major reheating event with over 200 °C temperature increase occurred just prior to the extrusive volcanic eruptions and this can be connected to the intrusion of hot basaltic magma into the felsic crystal mush body. This mantle-derived basaltic magma transported high-Mg olivines and clinopyroxenes into the silicic magma reservoir. The lack of strong resorbtion around many Mg-rich olivine and clinopyroxene crystals in the dacite implies that mixing of the mafic and silicic magma could occur just before the eruption. The melt-bearing crystal sponge was effectively remelted and as a consequence an eruptible magma was formed (Kiss et al., 2014). The key-elements in this process are the existence of a crystal mush body with some melt fraction, presumably not more then 10–20 vol.% and the ascent of a hot mafic magma batch, which had enough volume to reheat significant part of the cold magma body.

The mafic crystal clots in the Ciomadul dacite provide additional information about the deeper magma system. Clinopyroxenes often show compositional zoning including oscillatory zoning pattern with major changes in the mg-number and Cr content. This is consistent with intermittent replenishment in the mafic magma storage. Since we have no data on the melt composition equilibrated with the clinopyroxenes, it

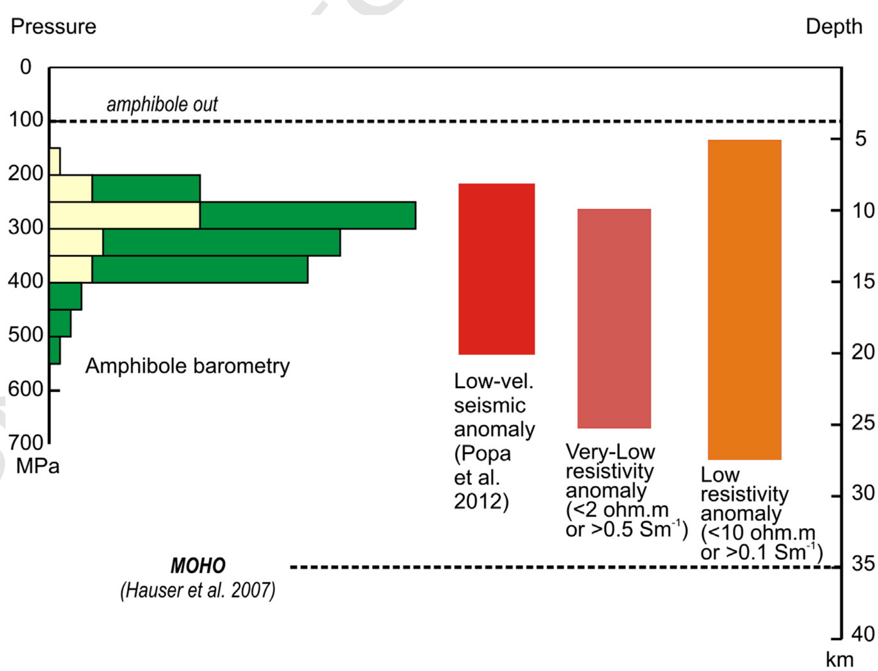

Fig. 11. Constrains on the depth of the magma chamber based on different methods: results of geobarometric calculations on the crystallization pressure of amphiboles (frequency distribution based on 121 amphibole compositional data; yellow: low-Al amphiboles; dark green: high-Al amphiboles; pressure values are obtained using the calculation scheme of Anderson et al. (2008) for low-Al amphiboles and Ridolfi et al. (2010) for high-Al amphiboles). The black dotted line denotes the stability limit of amphiboles in dacite magmas based on the experimental data of Blundy and Cashman (2001); low-velocity seismic anomaly based on the seismic tomography model of Popa et al. (2012); and the very low (<2 Ω m or >0.5 Sm^{-1}) and low resistivity anomaly (<10 Ω m or >0.1 Sm^{-1}) based on the 2D inversion model presented in this study (Fig. 8). The results of these independent techniques could imply the existence of a magmatic body with some melt fraction beneath Ciomadul at a depth range of 8–25 km. (For interpretation of the references to color in this figure legend, the reader is referred to the web version of this article.)

is not possible to estimate the depth of the mafic magma storage, but considering the thick crust (Rădulescu, 1988; Enescu et al., 1992; Dérerova et al., 2006) beneath the Ciomadul, we tentatively infer that this could be located at the crust–mantle boundary around 30–40 km depth.

8.2. Magnetotelluric indication for the magma storage

Magnetotelluric technique is a powerful tool to detect partially melted zone beneath volcanoes, since conductivity anomalies can be typically attributed to the presence of fluids, such as silicate melts in the crust and the mantle (Schilling et al., 1997, 2006; Baba et al., 2006; Heise et al., 2007; Hill et al., 2009; Pommier et al., 2010a; Pommier and Le-Trong, 2011). The high conductivity anomaly (0.2–0.8 Sm^{-1} in the strongest part) beneath Ciomadul at depth between 5 and 25 km obtained both from the 2D and 3D inversion modeling calculations (Figs. 8 and 9) clearly suggest interconnected fluids within the solid crustal rocks. At shallow depth, hydrothermally altered rocks and/or sedimentary deposits with interconnected pore fluids could explain the high conductivity values. Although we cannot entirely rule out the presence of aqueous fluid as being the cause of the high conductivity at greater depth, we think that the coherent high conductivity anomaly (0.3–0.8 Sm^{-1}) beneath 10 km (Fig. 8) can be more reliably explained by partially melted crustal zone. Partially melted zones with similar conductivity values were suggested by Schilling et al. (1997) and Brasse et al. (2002) beneath the Bolivian Altiplano, Hill et al. (2009) beneath Mt. St. Helens and Mt. Adams and Heise et al. (2007) beneath the Taupo Volcanic Zone. Pommier et al. (2010b) emphasized that electrical measurements in laboratories are important to distinguish whether the high conductivity indicates the presence of silicate melt or aqueous fluids. Brines (mineralized water) circulating in pores and fractures of the crustal rocks could have an extremely high conductivity (>1000 Sm^{-1}), whereas silicate melts have typically 0.01–10 Sm^{-1} electrical conductivity.

A partially melted zone consists of a two-phase medium with a solid rock matrix and interstitial melt. The bulk conductivity is controlled by the geometry of the melt fractions. Unconnected melt pockets in the resistive rock do not change significantly the bulk electrical behavior, whereas there is a noticeably increase in the conductivity in case of interconnected melt (Sato and Ida, 1984; Roberts and Tyburczy, 1999). Recently, it is emphasized that magma reservoirs even beneath active volcanoes are composed of mixture of crystals and melts in various proportions (crystal mush; Hildreth, 2004; Bachmann and Bergantz, 2004, 2008; Hildreth and Wilson, 2007). High conductivity in crustal level could thus indicate a crystal mush body with the presence of melt fraction in a critical amount that allows a sort of interconnection. The conductivity of a crystal mush zone with interconnected melt does not strongly depend on the solid rocks (Glover et al., 2000), but has a dependence on the composition of the melt phase, the pressure and temperature as well as on the relative amount of the melt within the electrically resistant solid framework (Pommier et al., 2008). The effect of temperature and pressure on the conductivity is described by an Arrhenius law and this was incorporated into the SIGMELT software developed by Pommier and Le-Trong (2011). Composition of the melt is a critical parameter to determine the conductivity, where Na_2O content has the most significant role (Gaillard, 2004; Pommier et al., 2008). Considering a dacitic melt with the typical composition of the Ciomadul volcanic rocks (Na_2O = 4.6 wt.%, SiO_2 = 64–67 wt.% and assuming 4 wt.% H_2O), the SIGMELT software (Pommier and Le-Trong, 2011) provides conductivity value of 0.5–1.1 Sm^{-1}, assuming 800–900 °C temperature and 200–300 MPa. However, if we consider a more residual melt fraction with higher SiO_2 content (>70 wt.%), the conductivity slightly decreases (0.1–0.2 Sm^{-1}). On the contrary, larger amount of dissolved water in the melt increases significantly the conductivity up to 6–8 Sm^{-1} at H_2O = 10 wt.%. The ubiquitous occurrence of hydrous phases (amphibole, biotite) in the Ciomadul dacites requires a water content >4 wt.% in the melt. Thus, we could infer that the melt conductivity at a dacitic to rhyolitic composition similar to that of the Ciomadul rocks could be around 1–1.5 Sm^{-1}, while 0.2–0.5 Sm^{-1} values could correspond with a partially melted zone containing 10–20% interconnected melt. This latter conductivity values fit well with the resistivity anomaly obtained by the 2D and 3D MT models at 5–25 km depth (Fig. 8).

9. Implications for a partially melted zone beneath Ciomadul

Our interpretation that a partially melted zone could result in the high conductive anomaly in the crust at 5–25 km is supported by other geophysical anomalies such as the seismic low velocity zone at the same depth (8–20 km; Popa et al., 2012) and the high heat flow (Demetrescu and Andreescu, 1994). Remarkably, the highest conductivity in the crustal level is detected just below the crater area. Furthermore, this is consistent with the recent volcanism of the Ciomadul. The petrologic constrains on the magma storage suggest the existence of silicic crystal mush between 7 and 14 km, where intrusion of basaltic magma could effectively remobilize it leading to volcanic eruption. Existence of a magmatic body is inferred also by the relatively high $^3He/^4He$ values (R_m/R_a is around 3.0–4.5) in the gases emanated at the Ciomadul (Vaselli et al., 2002). Furthermore, occurrence of Mg-rich and zoned clinopyroxenes requires a deeper magma chamber, possibly at the crust–mantle boundary. The 2D magnetotelluric models (Fig. 8) indicate a conductivity anomaly at 30–40 km slightly northeastward from the crater area that might fit with the petrologic assumption. Remarkably, the S-waves seismic tomographic profiles provided by Popa et al. (2012) also show a deeper low-velocity anomaly at same position.

Thus, the presence of a partially melted zone or with other words, a crystal mush body with some melt fraction beneath Ciomadul appears to be well established by independent observations. The inferred highest conductivity value (0.3–0.7 Sm^{-1}) from the 2D model of the MT measurements (Fig. 8) could indicate an interconnected network of highly conductive phases, i.e. melt in the crustal rocks. Considering a solid rock framework with conductivity of less than 0.01 Sm^{-1}, the melt fraction can be estimated following the method described by Schilling et al. (2006). Assuming melt conductivity calculated by the SIGMELT software (Pommier and Le-Trong, 2011) for a dacitic composition similar to the Ciomadul volcanic rocks (0.4–1.0 Sm^{-1}) a melt fraction of 5–15% is obtained. This can be regarded as a minimum value considering that some melt could be in isolated melt pocket (Partzsch et al., 2000).

The presence of a melt-bearing crystal mush body beneath Ciomadul would mean that there is a potential that this volcano might be rejuvenated in the future. Petrologic studies indicate that in the past (100–150 ka), volcanic eruptions were triggered by effective remobilization of an already locked, low temperature and low melt fraction silicic crystal mush via intrusion of hot basaltic magmas (Kiss et al., 2014). Such processes were invoked as a triggering mechanism for several similar volcanic systems (e.g., Unzen, Japan, Nakamura, 1995; Pinatubo, Philippines, Pallister et al., 1992; Soufriére Hills, Montserrat; Murphy et al., 2000). One of the key elements for such scenario is the presence of melt-bearing magmatic body beneath the volcano. This does not mean that Ciomadul is a potentially active volcano, since no unrest has been detected and no eruptions were documented in the last 10 ka. However, there are signs that volcanoes can be reactivated even after several 10s ka quiescence (Clynne and Muffler, 2010; Escobar-Wolf et al., 2010; Frey et al., 2013). Furthermore, inSAR and seismic data imply that the Uturuncu volcano in Bolivia, having last eruption at 270 ka, could have been replenished by fresh magma at the depth (Pritchard and Simons, 2002, 2004; Sparks et al., 2008). It is unclear whether this is just a magma storing episode or could lead to volcanic eruption in the future, however, it is a sign that deep magmatic processes could occur beneath a volcano well after the last volcanic eruptions. Furthermore, zircon geochronology on a number of locations shows

Please cite this article as: Harangi, S., et al., Combined magnetotelluric and petrologic constrains for the nature of the magma storage system beneath the Late Pleistocene Ciomadu..., J. Volcanol. Geotherm. Res. (2014), http://dx.doi.org/10.1016/j.jvolgeores.2014.12.006

that magmatic crystallization can be continuously taking place over several 10s or even >100s ka before the volcanic eruptions (e.g., Bachmann et al., 2007; Claiborne et al, 2010). Thus, we suggest for long-dormant or seemingly inactive volcanoes having melt-bearing magmatic body at depths to term as 'volcano with potentially active magma storage' or PAMS volcano. Although these volcanoes do not show presently clear sign of rejuvenation, future volcanic activity cannot be unambiguously excluded considering that the melt-bearing crystal mush body could potentially be remobilized. Thus, further combined petrologic and geophysical (e.g., further magnetotelluric) investigation as well as more focused gas-geochemical monitoring are necessary to refine the geometry and the state of the magma body beneath Ciomadul.

10. Uncited references

Harangi et al., 2013
Magyari et al., in press
Weaver et al., 2000

Acknowledgment

This research on the Ciomadul volcano belongs to the scientific project supported by the OTKA (Hungarian National Research Fund) No. K68587. Interpretation of the magnetotelluric data by A.N. was part of the János Bolyai Scholarship of the Hungarian Academy of Sciences and the TAMOP-4.2.2.C-11/1/KONV-2012-0015 (Earth-system) project sponsored by the EU and the European Social Foundation. Participation of the young scientists, Balázs Kiss and Réka Lukács in this research were supported by the European Union and the State of Hungary, co-financed by the European Social Fund in the framework of TÁMOP-4.2.4.A/ 2-11/1-2012-0001 'National Excellence Program'. We are grateful to Supercomputing Service of National Information Infrastructure Development Institute (Hungary) for support to calculation the 3-D modeling and inversion. We thank the Institute of Geodynamics, Romanian Academy for logistic support and Theo Ntaflos and Franz Kiraly (University of Vienna) for their help during the microprobe work. Ioan Seghedi was supported by grant of the Ministry of National Education, CNCS — UEFISCDI, project number PN-II-ID-PCE-2012-4-0137. Constructive comments provided by Károly Németh and an anonymous reviewer helped us to refine our views in the final version of the paper.

References

Ádám, A., Szarka, L., 2011. Geoelectromagnetism. In: Gupta, H.K. (Ed.), Encyclopedia of Solid Earth Geophysics. Springer, pp. 341–352.
Adam, J., Oberti, R., Cámara, F., Green, T.H., 2007. An electron microprobe, LAM-ICP-MS and single-crystal X-ray structure refinement study of the effects of pressure, melt-H_2O concentration and on experimentally produced basaltic amphiboles. Eur. J. Mineral. 19, 641–655.
Althaus, T., Niedermann, S., Erzinger, J., 2000. Noble gas studies of fluids and gas exhalations in the East Carpathians, Romania. Chem. Erde 60, 189–207.
Anderson, J.L., Smith, D.R., 1995. The effects of temperature and fO_2 on the Al-in-hornblende barometer. Am. Mineral. 80, 549–559.
Anderson, J.L., Barth, A.P., Wooden, J.L., Mazdab, F., 2008. Thermometers and thermobarometers in granitic systems. Rev. Mineral. Geochem. 69, 121–142.
Annen, C., Blundy, J.D., Sparks, R.S.J., 2006. The genesis of intermediate and silicic magmas in deep crustal hot zones. J. Petrol. 47, 505–539.
Baba, K., Chave, A.D., Evans, R.L., Hirth, G., Mackie, R., 2006. Mantle dynamics beneath the East Pacific Rise at 17S: insights from the Mantle Electromagnetic and Tomography (MELT) experiment. J. Geophys. Res. 111, B02101. http://dx.doi.org/10.1029/2004JB003598.
Bachmann, O., Bergantz, G.W., 2004. On the origin of crystal-poor rhyolites: extracted from batholithic crystal mushes. J. Petrol. 45, 1565–1582.
Bachmann, O., Bergantz, G.W., 2006. Gas percolation in upper-crustal magma bodies as a mechanism for upward heat advection and rejuvenation of silicic crystal mushes. J. Volcanol. Geotherm. Res. 149, 85–102.
Bachmann, O., Bergantz, G., 2008. The magma reservoirs that feed super eruptions. Elements 4, 17–21.
Bachmann, O., Dungan, M.A., 2002. Temperature-induced Al-zoning in hornblendes of the Fish Canyon magma, Colorado. Am. Mineral. 87, 1062–1076.
Bachmann, O., Charlier, B.L.A., Lowenstern, J.B., 2007. Zircon crystallization and recycling in the magma chamber of the rhyolitic Kos Plateau Tuff (Aegean arc). Geology 35, 73–76.
Bahr, K., 1988. Interpretation of the magnetotelluric impedance tensor: regional induction and local telluric distortion. J. Geophys. 62, 119–127.
Bahr, K., 1991. Geological noise in magnetotelluric data: a classification of distortion types. Phys. Earth Planet. Inter. 66, 24–38.
Barclay, J., Carmichael, I.S.E., 2004. A hornblende basalt from western Mexico: water-saturated phase relations constrain a pressure–temperature window of eruptibility. J. Petrol. 45, 485–506.
Blundy, J., Cashman, K., 2001. Ascent-driven crystallisation of dacite magmas at Mount St Helens, 1980–1986. Contrib. Mineral. Petrol. 140, 631–650.
Blundy, J.D., Holland, T.J.B., 1990. Calcic amphibole equilibria and a new amphibole-plagioclase geothermometer. Contrib. Mineral. Petrol. 104, 208–224.
Brasse, H., Lezaeta, P., Rath, V., Schwalenberg, K., Soyer, W., Haak, V., 2002. The Bolivian Altiplano conductivity anomaly. J. Geophys. Res. 107. http://dx.doi.org/10.1029/2001JB000391.
Burgisser, A., Bergantz, G.W., 2011. A rapid mechanism to remobilize and homogenize highly crystalline magma bodies. Nature 471, 212–215.
Caldwell, T.G., Bibby, H.M., Brown, C., 2004. The magnetotelluric phase tensor. Geophys. J. Int. 158, 457–469.
Cashman, K.V., Sparks, R.S.J., 2013. How volcanoes work: a 25 year perspective. Geol. Soc. Am. Bull. 125, 664–690.
Chalot-Prat, F., Gîrbacea, R., 2000. Partial delamination of continental mantle lithosphere, uplift-related crust-mantle decoupling, volcanism and basin formation: a new model for the Pliocene–Quaternary evolution of the southern East-Carpathians, Romania. Tectonophysics 327, 83–107.
Chambefort, I., Dilles, J.H., Longo, A.A., 2013. Amphibole geochemistry of the Yanacocha volcanics, Peru: evidence for diverse sources of magmatic volatiles related to gold ores. J. Petrol. 54, 1017–1046.
Claiborne, L.L., Miller, C.F., Flanagan, D.M., Clynne, M.A., Wooden, J.L., 2010. Zircon reveals protracted magma storage and recycling beneath Mount St. Helens. Geology 38, 1011–1014.
Cloetingh, S.A.P.L., Burov, E., Matenco, L., Toussaint, G., Bertotti, G., Andriessen, P.A.M., Wortel, M.J.R., Spakman, W., 2004. Thermo-mechanical controls on the mode of continental collision in the SE Carpathians (Romania). Earth Planet. Sci. Lett. 218, 57–76.
Clynne, M.A., Muffler, L.J.P., 2010. Geologic Map of Lassen Volcanic National Park and Vicinity, California. U.S. Geological Survey Scientific Investigations Map 2899, p. 110.
Clynne, M.A., Calvert, A.T., Wolfe, E.W., Evarts, R.C., Fleck, R.J., Lanphere, M.A., 2008. The Pleistocene eruptive history of Mount St. Helens, Washington, from 300,000 to 12,000 years before present. In: Sherrod, D.R. (Ed.), A Volcano Rekindled; the Renewed Eruption of Mount St. Helens, 2004–2006. U.S. Geological Survey Professional Paper 1750, pp. 593–627.
Coombs, M.L., Sisson, T.W., Bleick, H.A., Henton, S.M., Nye, C.J., Payne, A.L., Cameron, C.E., Larsen, J.F., Wallace, K.L., Bull, K.F., 2013. Andesites of the 2009 eruption of Redoubt Volcano, Alaska. J. Volcanol. Geotherm. Res. 259, 349–372.
Cooper, K.M., Kent, A.J.R., 2014. Rapid remobilization of magmatic crystals kept in cold storage. Nature 506, 480–483.
Costa, F., Andreastuti, S., Bouvet de Maisonneuve, C., Pallister, J.S., 2013. Petrological insights into the storage conditions, and magmatic processes that yielded the centennial 2010 Merapi explosive eruption. J. Volcanol. Geotherm. Res. 261, 209–235.
Demetrescu, C., Andreescu, M., 1994. On the thermal regime of some tectonic units in a continental collision environment in Romania. Tectonophysics 230, 265–276.
Dérerova, J., Zeyen, H., Bielik, M., Salman, K., 2006. Application of integrated geophysical modeling for determination of the continental lithospheric thermal structure in the Eastern Carpathians. Tectonics 25, TC3009.
Desissa, M., Johnson, N.E., Whaler, K.A., Hautot, S., Fisseha, S., Dawes, G.J.K., 2013. A mantle magma reservoir beneath an incipient mid-ocean ridge in Afar, Ethiopia. Nat. Geosci. 6, 861–865.
Díaz, D., Brasse, H., Ticona, F., 2012. Conductivity distribution beneath Lascar volcano (Northern Chile) and the Puna, inferred from magnetotelluric data. J. Volcanol. Geotherm. Res. 217–218, 21–29.
Egbert, G.D., Booker, J.R., 1986. Robust estimation of geomagnetic transfer functions. Geophys. J. R. Astron. Soc. 87, 173–194.
Egbert, G.D., Livelybrooks, D.W., 1996. Single station magnetotelluric impedance estimation: coherence weighting and the regression M-estimate. Geophysics 61, 964–970.
Enescu, D., Danchiv, D., Bala, A., 1992. Lithosphere structure in Romania II. Thickness of the Earth crust. Depth-dependent propagation velocity curves for the P and S waves. Stud. Cercet. Geol. Geofiz. Geogr. Ser. Geofiz. 30, 3–19.
Erdmann, S., Martel, C., Pichavant, M., Kushnir, A., 2014. Amphibole as an archivist of magmatic crystallization conditions: problems, potential, and implications for inferring magma storage prior to the paroxysmal 2010 eruption of Mount Merapi, Indonesia. Contrib. Mineral. Petrol. 167, 1016.
Escobar-Wolf, R.P., Diehl, J.F., Singer, B.S., Rose, W.I., 2010. $^{40}Ar/^{39}Ar$ and paleomagnetic constraints on the evolution of Volcán de Santa María, Guatemala. Geol. Soc. Am. Bull. 122, 757–771.
Fillerup, M.A., Knapp, J.H., Knapp, C.C., Raileanu, V., 2010. Mantle earthquakes in the absence of subduction? Continental delamination in the Romanian Carpathians. Lithosphere 2, 333–340.
Frey, H.M., Lange, R.A., Hall, C.M., Nelson, S.A., Delgado-Granados, H., Mastin, L., Wineberg, D., 2013. $^{40}Ar/^{39}Ar$ geochronology of Volcán Tepetiltic, western Mexico: Implications for the origin of zoned rhyodacite–rhyolite liquid erupted explosively from an andesite stratovolcano after a prolonged hiatus. Geol. Soc. Am. Bull. B30790.1.
Gaillard, F., 2004. Laboratory measurements of electrical conductivity of hydrous and dry silicic melts under pressure. Earth Planet. Sci. Lett. 218, 215–228.

Please cite this article as: Harangi, S., et al., Combined magnetotelluric and petrologic constrains for the nature of the magma storage system beneath the Late Pleistocene Ciomadu..., J. Volcanol. Geotherm. Res. (2014), http://dx.doi.org/10.1016/j.jvolgeores.2014.12.006

Gîrbacea, R., Frisch, W., 1998. Slab in the wrong place: lower lithospheric mantle delamination in the last stage of the Eastern Carpathian subduction retreat. Geology 26, 611–614.

Glover, P.W.J., Hole, M.J., Pous, J., 2000. A modified Archie's law for two conducting phases. Earth Planet. Sci. Lett. 180, 369–383.

Hammarstrom, J.M., Zen, E., 1986. Aluminum in hornblende; an empirical igneous geobarometer. Am. Mineral. 71, 1297–1313.

Harangi, S., 2007. A Kárpát-Pannon térség legutolsó vulkáni kitörései - lesz-e még folytatás? (The last volcanic eruptions in the Carpathian–Pannonian Region — to be continued?). Földr. Közl. 131, 271–288.

Harangi, Sz, Molnár, M., Vinkler, A.P., Kiss, B., Jull, A.J.T., Leonard, A.E., 2010. Radiocarbon dating of the last volcanic eruptions of Ciomadul volcano, Southeast Carpathians, eastern–central Europe. Radiocarbon 52, 1498–1507.

Harangi, S., Sági, T., Seghedi, I., Ntaflos, T., 2013. A combined whole-rock and mineral-scale investigation to reveal the origin of the basaltic magmas of the Perşani monogenetic volcanic field, Romania, eastern–central Europe. Lithos 180–181, 43–57.

Heise, W., Bibby, H.M., Caldwell, T.G., Bannister, S.C., Ogawa, Y., Takakura, S., Uchida, T., 2007. Melt distribution beneath a young continental rift: the Taupo Volcanic Zone, New Zealand. Geophys. Res. Lett. 34, L14313. http://dx.doi.org/10.1029/2007GL029629.

Hildreth, W., 1981. Gradients in silicic magma chambers: implications for lithospheric magmatism. J. Geophys. Res. 86, 10153–10192.

Hildreth, W., 2004. Volcanological perspectives on Long Valley, Mammoth Mountain, and Mono Craters: several contiguous but discrete systems. J. Volcanol. Geotherm. Res. 136, 169–198.

Hildreth, W., Wilson, C.J.N., 2007. Compositional zoning of the Bishop Tuff. J. Petrol. 48, 951–999.

Hill, G.J., Caldwell, T.G., Heise, W., Chertkoff, D.G., Bibby, H.M., Burgess, M.K., Cull, J.P., Cas, R.A.F., 2009. Distribution of melt beneath Mount St Helens and Mount Adams inferred from magnetotelluric data. Nat. Geosci. 2, 785–789.

Holtz, F., Johannes, W., Tamic, N., Behrens, H., 2001. Maximum and minimum water contents of granitic melts generated in the crust: a re-evaluation and implications. Lithos 56, 1–14.

Huber, C., Bachmann, O., Dufek, J., 2011. Thermo-mechanical reactivation of locked crystal mushes: melting-induced internal fracturation and assimilation processes in magmas. Earth Planet. Sci. Lett. 304, 443–454.

Humphreys, M.C.S., Blundy, J.D., Sparks, R.S.J., 2006. Magma evolution and open-system processes at Shiveluch volcano: insights from phenocryst zoning. J. Petrol. 47, 2303–2334.

Ingham, M.R., 1988. A magnetotelluric and magnetovariational traverse across the New Zealand subduction zone. Geophys. J. 92, 495–504.

Ingham, M.R., 2005. Deep electrical structure of the Central Volcanic Region and Taupo Volcanic Zone, New Zealand. Earth Planets Space 57, 591–603.

Ingham, M.R., Bibby, H.M., Heise, W., Jones, K.A., Cairns, P., Dravitzki, S., Bennie, S.L., Caldwell, T.G., Ogawa, Y., 2009. A magnetotelluric study of Mount Ruapehu volcano, New Zealand. Geophys. J. Int. 179, 887–904.

Johnson, M.C., Rutherford, M.J., 1989. Experimental calibration of the aluminum-in-hornblende geobarometer with application to Long Valley caldera (California) volcanic rocks. Geology 17, 837–841.

Karátson, D., Telbisz, T., Harangi, S., Magyari, E., Dunkl, I., Kiss, B., Jánosi, C., Veres, D., Braun, M., Fodor, E., Biró, T., Kósik, S., von Eynatten, H., Lin, D., 2013. Morphometrical and geochronological constraints on the youngest eruptive activity in East–Central Europe at the Ciomadul (Csomád) lava dome complex, East Carpathians. J. Volcanol. Geotherm. Res. 255, 43–56.

Kiss, B., Harangi, S., Ntaflos, T., Mason, P.R.D., Pál-Molnár, E., 2014. Amphibole perspective to unravel pre-eruptive processes and conditions in volcanic plumbing systems beneath intermediate arc volcanoes: a case study from Ciomadul volcano (SE Carpathians). Contrib. Mineral. Petrol. 167, 986. http://dx.doi.org/10.1007/s00410-014-0986-6.

Koulakov, I., Zaharia, B., Enescu, B., Radulian, M., Popa, M., Parolai, S., Zschau, J., 2010. Delamination or slab detachment beneath Vrancea? New arguments from local earthquake tomography. Geochem. Geophys. Geosyst. 11, Q03002.

Lorinczi, P., Houseman, G.A., 2009. Lithospheric gravitational instability beneath the Southeast Carpathians. Tectonophysics 474, 322–336.

Magyari, E., Buczkó, K., Jakab, G., Braun, M., Pál, Z., Karátson, D., Pap, I., 2009. Palaeolimnology of the last crater lake in the Eastern Carpathian Mountains: a multiproxy study of Holocene hydrological changes. Hydrobiologia 631, 29–63.

Magyari, E.K., Veres, D., Wennrich, V., Wagner, B., Braun, M., Karátson, D., Pál, Z., Ferenczy, Gy, St-Onge, G., Rethmayer, J., Francois, J.-P., Schäbitz, F., 2014. Vegetation and environmental responses to climate forcing during the last glacial maximum and deglaciation in the Romanian Carpathians: attenuated response to maximum cooling and increased biomass burning. Quat. Sci. Rev. (in press).

Martin, M., Wenzel, F., CALIXTO Working Group, 2006. High-resolution teleseismic body wave tomography beneath SE Romania: II. Imaging of a slab detachment scenario. Geophys. J. Int. 164, 579–595.

Mason, P.R.D., Downes, H., Seghedi, I., Szakács, A., Thirlwall, M.F., 1995. Low-pressure evolution of magmas from the Calimani, Gurghiu and Hargita Mountains, East Carpathians. Acta Vulcanol. 7, 43–52.

Mason, P.R.D., Downes, H., Thirlwall, M., Seghedi, I., Szakács, A., Lowry, D., Mattey, D., 1996. Crustal assimilation as a major petrogenetic process in the East Carpathian Neogene and Quaternary continental margin arc, Romania. J. Petrol. 37, 927–959.

Mason, P.R.D., Seghedi, I., Szakács, A., Downes, H., 1998. Magmatic constraints on geodynamic models of subduction int he East Carpathians, Romania. Tectonophysics 297, 157–176.

Matsushima, N., Oshima, H., Ogawa, Y., Takakura, S., Satoh, H., Utsugi, M., Nishida, Y., 2001. Magma prospecting in Usu volcano, Hokkaido, Japan, using magnetotelluric soundings. J. Volcanol. Geotherm. Res. 109, 263–277.

Moriya, I., Okuno, M., Nakamura, T., Ono, K., Szakács, A., Seghedi, I., 1996. Radiocarbon Ages of Charcoal Fragments from the Pumice Flow Deposits of the Last Eruption of Ciomadul Volcano, Romania. Summaries of Research Using AMS at Nagoya University VII pp. 255–257.

Murphy, M.D., Sparks, R.S.J., Barclay, J., Caroll, M.R., Brewer, T.S., 2000. Remobilization of andesite magma by intrusion of mafic magma at the Soufriere Hills volcano, Montserrat, West Indies. J. Petrol. 41, 21–42.

Nakamura, M., 1995. Continuous mixing of crystal mush and replenished magma in the ongoing Unzen eruption. Geology 23, 807–810.

Newman, G.A., Wannamaker, P.E., Hohmann, G.W., 1985. On the detectability of crustal magma chambers using the magnetotelluric method. Geophysics 50, 1136–1143.

Oncescu, M.C., Burlacu, V., Anghel, M., Smalberger, V., 1984. Three-dimensional P-wave velocity image under the Carpathian arc. Tectonophysics 106, 305–319.

Pallister, J.S., Hoblitt, R.P., Reyes, A.G., 1992. A basalt trigger for the 1991 eruptions of Pinatubo volcano? Nature 356, 426–428.

Pallister, J.S., Hoblitt, R.P., Meeker, G.P., Knight, R.J., Siems, D.F., 1996. Magma mixing at Mount Pinatubo: petrographic and chemical evidence from the 1991 deposits. In: Newhall, C.G., Punongbayan, R.S. (Eds.), Fire and Mud: Eruptions and Lahars of Mount Pinatubo, Philippines, Seattle and London, pp. 687–731.

Park, S.K., Ostos, L.C., 2013. Constraints from magnetotelluric measurements on magmatic processes and upper mantle structure in the vicinity of Lassen volcanic center, northern California. Geosphere 9, 382–393.

Partzsch, G.M., Schilling, F.R., Arndt, J., 2000. The influence of partial melting on the electrical behavior of crustal rocks: laboratory examinations, model calculations and geological interpretations. Tectonophysics 317, 189–203.

Pécskay, Z., Szakács, A., Seghedi, I., Karátson, D., 1992. Contributions to the geochronology of Mt. Cucu volcano and the South Harghita (East Carpathians, Romania). Földtani Közlöny (Bull. Hung. Geol. Soc.) 122, 265–286.

Pécskay, Z., Edelstein, O., Seghedi, I., Szakacs, A., Kovacs, M., Crihan, M., Bernad, A., 1995. K_Ar datings of Neogene–Quaternary calc-alkaline volcanic rocks in Romania. Acta Vulcanol. 7, 53–61.

Peltz, S., Vajdea, E., Balogh, K., Pécskay, Z., 1987. Contribution to the geochronological study of the volcanic processes in the Calimani and Harghita Mts. Dari de Seama ale Sedintelor Institutul de Geologie si Geofizica 72–73pp. 323–338.

Pichavant, M., Martel, C., Bourdier, J.-L., Scaillet, B., 2002. Physical conditions, structure, and dynamics of a zoned magma chamber: Mount Pelée (Martinique, Lesser Antilles Arc). J. Geophys. Res. 107, 1–28.

Pommier, A., Le-Trong, E., 2011. “SIGMELTS”: a web portal for electrical conductivity calculations in geosciences. Comp. Geosci. 37, 1450–1459.

Pommier, A., Gaillard, F., Pichavant, M., Scaillet, B., 2008. Laboratory measurements of electrical conductivities of hydrous and dry Mount Vesuvius melts under pressure. J. Geophys. Res. 113, B05205. http://dx.doi.org/10.1029/2007JB005269.

Pommier, A., Gaillard, F., Malki, M., Pichavant, M., 2010a. Re-evaluation of the electrical conductivity of silicate melts. Am. Mineral. 95, 284–291.

Pommier, A., Tarits, P., Hautot, S., Pichavant, M., Scaillet, B., Gaillard, F., 2010b. A new petrological and geophysical investigation of the present-day plumbing system of Mount Vesuvius. Geochem. Geophys. Geosyst. 11. http://dx.doi.org/10.1029/2010GC003059.

Popa, M., Radulian, M., Szakács, A., Seghedi, I., Zaharia, B., 2012. New seismic and tomography data in the southern part of the Harghita Mountains (Romania, Southeastern Carpathians): connection with recent volcanic activity. Pure Appl. Geophys. 169, 1557–1573.

Pritchard, M.E., Simons, M., 2002. A satellite geodetic survey of large-scale deformation of volcanic centres in the central Andes. Nature 418, 167–171.

Pritchard, M.E., Simons, M., 2004. An InSAR-based survey of volcanic deformation in the central Andes. Geochem. Geophys. Geosyst. 5. http://dx.doi.org/10.1029/2003GC000610.

Rădulescu, F., 1988. Seismic models of the crustal structure in Romania. Rev. Roum. Géol. Géophys. Géogr. Sér. Géophys. 32, 13–17.

Rădulescu, D., Péter, E., Stanciu, C., Ştefănescu, M., Veliciu, Ş., 1981. On the geothermic anomalies in the southern part of Harghita Mts. (Asupra anomaliilor geotermice din sudul munţilor Harghita. Consideratii pe marginea unor prime cercetări). St. Cerc. de Geol., Geof., Geogr., seria Geologie, T26/2pp. 168–184 (Bucureşti (in Romanian)).

Ren, Y., Stuart, G.W., Houseman, G.A., Dando, B., Ionescu, C., Hegedüs, E., Radovanović, S., Shen, Y., 2012. Upper mantle structures beneath the Carpathian–Pannonian region: implications for the geodynamics of continental collision. Earth Planet. Sci. Lett. 349–350, 139–152.

Ridolfi, F., Renzulli, A., 2012. Calcic amphiboles in calc-alkaline and alkaline magmas: thermobarometric and chemometric empirical equations valid up to 1,130 °C and 2.2 GPa. Contrib. Mineral. Petrol. 163, 877–895.

Ridolfi, F., Renzulli, A., Puerini, M., 2010. Stability and chemical equilibrium of amphibole in calc-alkaline magmas: an overview, new thermobarometric formulations and application to subduction-related volcanoes. Contrib. Mineral. Petrol. 160, 45–66.

Roberts, J.J., Tyburczy, J.A., 1999. Partial-melt electrical conductivity: influence of melt composition. J. Geophys. Res. 104, 7055–7065.

Rodi, W.L., Mackie, R.L., 2001. Nonlinear conjugate gradients algorithm for 2-D magnetotelluric inversion. Geophysics 66, 174–187.

Sato, H., Ida, Y., 1984. Low-frequency electrical-impedance of partial melt geometry on electrical properties. Tectonophysics 107, 103–134.

Sato, H., Holtz, F., Behrens, H., Botcharnikov, R., Nakada, S., 2005. Experimental petrology of the 1991–1995 Unzen dacite, Japan. Part II: Cl/OH partitioning between hornblende and melt and its implications for the origin of oscillatory zoning of hornblende phenocrysts. J. Petrol. 46, 339–354.

Schilling, F.R., Partzsch, G.M., Brasse, H., Schwarz, G., 1997. Partial melting below the magmatic arc in the central Andes deduced from geoelectromagnetic field experiments and laboratory data. Phys. Earth Planet. Inter. 103, 17–32.

Schilling, F.R., Trumbull, R.B., Brasse, H., Haberland, C., Asch, G., Bruhn, D., Mai, K., Haak, V., Giese, P., Munoz, M., Ramelow, J., Rietbrock, A., Ricaldi, E., Vietor, T., 2006. Partial melting in the Central Andean crust: a review of geophysical, petrophysical, and petrologic evidence. In: Oncken, O., et al. (Eds.), The Andes: Active Subduction Orogeny. Frontiers in Earth Sciences. Springer-Verlag, Berlin-Heidelberg, pp. 459–474.

Schmidt, M.W., 1992. Amphibole composition in tonalite as a function of pressure: an experimental calibration of the Al-in-hornblende barometer. Contrib. Mineral. Petrol. 110, 304–310.

Scott, J.A.J., Mather, T.A., Pyle, D.M., Rose, W.I., Chigna, G., 2012. The magmatic plumbing system beneath Santiaguito Volcano, Guatemala. J. Volcanol. Geotherm. Res. 237–238, 54–68.

Seghedi, I., Szakács, A., Udrescu, C., Stoian, M., Grabari, G., 1987. Trace element geochemistry of the South Hargitha volcanics (East Carpathians): calc-alkaline and shoshonitic association. Dari S. Sed. Inst. Geol. Geofiz. 72–73, 381–397.

Seghedi, I., Maţenco, L., Downes, H., Mason, P.R.D., Szakács, A., Pécskay, Z., 2011. Tectonic significance of changes in post-subduction Pliocene–Quaternary magmatism in the south east part of the Carpathian–Pannonian Region. Tectonophysics 502, 146–157.

Shane, P., Smith, V.C., 2013. Using amphibole crystals to reconstruct magma storage temperatures and pressures for the post-caldera collapse volcanism at Okataina volcano. Lithos 156–159, 159–170.

Shcherbakov, V.D., Plechov, P.Y., Izbekov, P.E., Shipman, J.S., 2011. Plagioclase zoning as an indicator of magma processes at Bezymianny Volcano, Kamchatka. Contrib. Mineral. Petrol. 162, 83–99.

Siebert, L., Simkin, T., Kimberly, P., 2011. Volcanoes of the World. 3rd edition. Univ California Press, Berkeley (568 pp.).

Siripurnvaraporn, W., Egbert, G., 2000. An efficient data-subspace inversion method for two-dimensional magnetotelluric data. Geophysics 65, 791–803.

Siripurnvaraporn, W., Egbert, G., Lenbury, Y., Uyeshime, M., 2005a. Three-dimensional magnetotelluric: data space method. Phys. Earth Planet. Inter. 150, 3–14.

Siripurnvaraporn, W., Egbert, G., Uyeshime, M., 2005b. Interpretation of two-dimensional magnetotelluric profile data with three-dimensional inversion: synthetic examples. Geophys. J. Int. 160, 804–814.

Sparks, R.S.J., Folkes, C.B., Humphreys, M.C.S., Barfod, D.N., Clavero, J., Sunagua, M.C., McNutt, S.R., Pritchard, M.E., 2008. Uturuncu volcano, Bolivia: volcanic unrest due to mid-crustal magma intrusion. Am. J. Sci. 308, 727–769.

Sperner, B., Lorenz, F., Bonjer, K., Hettel, S., Muller, B., Wenzel, F., 2001. Slab break-off — abrupt cut or gradual detachment? New insights from the Vrancea Region (SE Carpathians, Romania). Terra Nova 13, 172–179.

Spichak, V.V., 2012. Evaluation of the feasibility of recovering the magma chamber's parameters by 3D Bayesian statistical inversion of synthetic MT data. Acta Geophys. 60, 942–958.

Stroncik, N.A., Klügel, A., Hansteen, T.H., 2009. The magmatic plumbing system beneath El Hierro (Canary Islands): constraints from phenocrysts and naturally quenched basaltic glasses in submarine rocks. Contrib. Mineral. Petrol. 157, 593–607.

Swift, C.M., 1967. Magnetotelluric Investigation of an Electrical Conductivity Anomaly in the Southwestern United States. (PhD thesis), Department of Geology and Geophysics, MIT, Cambridge, MA (reprinted in Magnetotelluric Methods, pp. 156–166, ed. Vozoff, K., Geophys. Reprint Ser. No. 5. 1988, SEG, Tulsa, OK).

Szakács, A., Seghedi, I., 1986. Chemical diagnosis of the volcanics from the most southernmost part of the Harghita Mountains—proposal for a new nomenclature. Rev. Roum. Géol. Géophys. Géogr. Géol. 30, 41–48.

Szakács, A., Seghedi, I., 1995. The Călimani–Gurghiu–Harghita volcanic chain, East Carpathians, Romania: volcanological features. Acta Volcanol. 7, 145–155.

Szakács, A., Seghedi, I., 2013. The relevance of volcanic hazard in Romania: is there any? Environ. Eng. Manag. J. 12, 125–135.

Szakács, A., Seghedi, I., Pécskay, Z., 1993. Peculiarities of South Harghita Mts. as terminal segment of the Carpathian Neogene to Quaternary volcanic chain. Rev. Roum. Géol. Géophys. Géogr. Géol. 37, 21–37.

Szakács, A., Seghedi, I., Pécskay, Z., 2002. The most recent volcanism in the Carpathian–Pannonian Region. Is there any volcanic hazard? Geol. Carpath. 193–194.

Turner, S.J., Izbekov, P., Langmuir, C., 2013. The magma plumbing system of Bezymianny Volcano: insights from a 54 year time series of trace element whole-rock geochemistry and amphibole compositions. J. Volcanol. Geotherm. Res. 263, 108–121.

Umeda, K., Asamori, K., Negi, T., Ogawa, Y., 2006. Magnetotelluric imaging of crustal magma storage beneath the Mesozoic crystalline mountains in a nonvolcanic region, northeast Japan. Geochem. Geophys. Geosyst. 7, Q08005. http://dx.doi.org/10.1029/2006GC001247.

Vaselli, O., Minissale, A., Tassi, F., Magro, G., Seghedi, I., Ioane, D., Szakács, A., 2002. A geochemical traverse across the Eastern Carpathians (Romania): constraints on the origin and evolution of the mineral water and gas discharges. Chem. Geol. 182, 637–654.

Verő, J., 1972. On the determination of the magnetotelluric impedance tensor. Acta Geodaet. Geophys. Montanist. Hung. 7, 333–351.

Viccaro, M., Giuffrida, M., Nicotra, E., Ozerov, A.Y., 2012. Magma storage, ascent and recharge history prior to the 1991 eruption at Avachinsky Volcano, Kamchatka, Russia: inferences on the plumbing system geometry. Lithos 140, 11–24.

Vinkler, A.P., Harangi, S., Ntaflos, T., Szakács, A., 2007. A Csomád vulkán (Keleti-Kárpátok) horzsaköveinek kőzettani és geokémiai vizsgálata – petrogenetikai következtetések (Petrology and geochemistry of pumices from the Ciomadul volcano (Eastern Carpathians) — implications for petrogenetic processes). Földt. Közl. (Bull. Hung. Geol. Soc.) 137, 103–128.

Walker Jr., B., Klemetti, E., Grunder, A., Dilles, J., Tepley, F., Giles, D., 2013. Crystal reaming during the assembly, maturation, and waning of an eleven-million-year crustal magma cycle: thermobarometry of the Aucanquilcha Volcanic Cluster. Contrib. Mineral. Petrol. 165, 663–682.

Wannamaker, P.E., Hasterok, D.P., Johnston, J.M., Stodt, J.A., Hall, D.B., Sodergren, T.L., Pellerin, L., Maris, V., Doerner, W.M., Groenewold, K.A., Unsworth, M.J., 2008. Lithospheric dismemberment and magmatic processes of the Great Basin–Colorado Plateau transition, Utah, implied from magnetotellurics. Geochem. Geophys. Geosyst. 9, 1–38.

Weaver, J.T., Agarwal, A.K., Lilley, F.E.M., 2000. Characterization of the magnetotelluric tensor in terms of its invariants. Geophys. J. Int. 141, 321–337.

Wenzel, F., Lorenz, F., Sperner, B., Oncescu, M.C., 1999. Seismotectonics of the Romanian Vrancea area. In: Wenzel, F., Lungu, D., Novak, O. (Eds.), Vrancea Earthquakes: Tectonics, Hazard and Risk Mitigation. Kluwer Academic Publishers, Dordrecht, pp. 15–26.

Wiese, H., 1962. Geomagnetisch Teiefentellurik 2, Die Streichrichtundger Untergrundstrukturen des elektrischen Widerstandes, erschlossen aus geomagnetische Variationen. Geofis. Pura Appl. 52, 83.